



OPEN Quantitative reconstruction of phase states and evolution of condensate and gas in the western Kelasu Thrust Belt, Kuqa Depression, Tarim Basin

Zhihua He^{1,2}, Chengsheng Chen¹✉, Chao Wu³, Shuyong Shi¹, Tao Mo³, Min Liu^{1,2}, Naidong Chen³ & Yunpeng Wang¹✉

Various oil-gas reservoirs have been discovered in the Lower Cretaceous Beshijiqike Formation in the western Kelasu Thrust Belt, Kuqa Depression, Tarim Basin. However, uncertain evolutionary characteristics, physical properties, and formation process for diverse phase states hinder further petroleum exploration and development. In this study, we reconstructed models of phase state evolution of six wells integrating PVT simulation and basin modeling. The results indicated that the temperature and pressure of reservoirs increased slowly before the Neogene, and then rapidly reached present value. The density and viscosity of the liquid phase decreased gradually, whereas that of the gas phase to the contrary. The reservoir fluids of all wells except for well DB-302 experienced phase differentiation, changing from gas-liquid coexistence phase (GLCP) to liquid or condensate phase. Three evolutionary pathways for the reservoir fluids represent three distinct scenarios: (1) Transition from GLCP to liquid phase, resulting from the reservoir formation mechanism by mainly early oil charge with no or minor late gas charge. (2) Transition from GLCP to condensate phase, resulting from the reservoir formation mechanism by early oil charge and subsequent gas charge. (3) Continuous maintenance in the gas phase, resulting from the reservoir formation mechanism by a large amount of late gas charge with no or very small amount of early oil charge. We proposed a pattern of two early stages of oil-filling followed by a later gas-charging stage, and suggested faults and covariations of trap formation timing with main hydrocarbon generation period are the main factors controlling phase states of the study area. Our results are significant for predicting fluid phase state of the study area.

Keywords PVT simulation, Basin modeling, Tectonic compression, Reservoir trap formation, Hydrocarbons accumulation process

The Kuqa Depression is an important petroliferous area and recorded the earliest gas field discovery in the Tarim Basin, western China^{1,2}. A series of thrust fault-related folds form the major traps in the depression, leading to the Kelasu Thrust Belt (KTB; Fig. 1) being a favorable area for hydrocarbon accumulations³. For instance, the Kela-2 and the Keshen giant gas fields were discovered in the eastern KTB respectively in 1998 and 2008^{4,5}. In recent years, consistent exploration breakthroughs in the western KTB have revealed a huge oil and gas production area in the Bozi-Dabei area^{6,7}. Oil and gas reservoirs of different phase states have been discovered in this area.

It is generally accepted that the phase state of a fluid is determined by its chemical composition and the reservoir conditions (temperature and pressure). The chemical composition is determined by the maturity of the source rock and the charging history of oil and gas, while tectonic evolution and structural adjustments have a profound impact on the reservoir temperature and pressure. It was found that hydrocarbon fluids in the KTB are generally controlled by a distribution of blocks divided from east to west, and belts divided from

¹State Key Laboratory of Deep Earth Processes and Resources, Guangzhou Institute of Geochemistry, Chinese Academy of Sciences, Guangzhou 510640, China. ²University of Chinese Academy of Sciences, Beijing 100049, China. ³Research Institute of Petroleum Exploration and Development, Tarim Oilfield Company, PetroChina, Korla 841000, China. ✉email: chenchengsheng@gig.ac.cn; wangyp@gig.ac.cn

north to south⁸ (Fig. 1). As shown in the Fig. 1e, four types of oil and gas reservoirs, classified based on their production gas-oil ratio and gas dryness coefficient, exhibit a circular spatial distribution pattern. Volatile oil and condensate reservoirs are predominantly located in the southern and northern parts of the Bozi segment, while wet gas and dry gas reservoirs are concentrated toward the central portion of the Bozi-Dabei area (Fig. 1e). However, previous studies mainly focussed on the characteristics of the phase state of oil and gas in single wells under current conditions^{9,10}. Few studies have considered the evolutionary characteristics of the phase state in KTB reservoirs under different temperature and pressure conditions, and the influence of tectonic movements on the phase state.

The western KTB experienced intense tectonic deformation and rapid sedimentation after the Neogene^{11,12}. Thrust folds and faults are widely developed, and provide the necessary conditions for the migration and accumulation of oil and gas. Oil and gas reservoirs in the KTB are characterised by deep burial, high temperatures, and overpressure¹³. Generally, present depth of burial of the Lower Cretaceous Bashijiqike Formation (K_1bs) is more than 5000 m¹⁴. The lack of understanding of the evolution of the phase states of the reservoirs and the main controlling factors under such a complex geological setting is an urgent problem, which currently hinders further exploration and development targeting deep strata in the western KTB.

To address this critical problem, we take a quantitative approach to reconstruct the changes in phase states of the reservoir fluids over time. In this paper, we studied the phase characteristics and evolutionary process of fluids in six wells: BZ-7, BZ-13, DB-1401, BZ-17, DB-17 and DB-302. These wells contain four types of petroleum: a volatile oil reservoir in BZ-7; condensate reservoirs in BZ-13 and DB-1401; wet gas reservoirs in BZ-17 and DB-17; and a dry gas reservoir in DB-302. The phase characteristics of fluids in these wells were simulated by PVTsim software which produced reliable fluid phase diagrams, and the burial, temperature, pressure histories of the reservoir strata were modelled by PetroMod (1D) software. We studied the evolution of the different in-situ fluid phases, including their density and viscosity under ideal conditions, by integrating the results of the PVTsim and the PetroMod software, with the aim of providing a comprehensive understanding of such fluids under a thrust setting, so as to aid petroleum exploration. The main controlling factors and evolutionary patterns of the fluid phase states were analyzed and summarized.

Geological setting

The Kuqa Depression is a secondary unit between the South Tianshan Mountains and the Tabei Uplift, and is strategically located along the northern margin of the Tarim Basin in northwestern China, following an NE-SW trend (Fig. 1a). The depression spans approximately 550 km in length from east to west, and varies between 30 km and 80 km in width from north to south^{4,15}. Tectonically, the Kuqa Depression is divided into the Northern Monocline Belt, the Kelasu-Yiqikelike Thrust Belt, the Baicheng and Yangxia Sags, the Qiulitage Thrust Belt, and the Southern Gentle Slope¹⁶ (Fig. 1b).

The KTB (Fig. 1b) is considered one of the most favorable areas for hydrocarbon accumulation in the northern Tarim Basin^{4,16}. Based on the development of traps, the belt is divided into five segments from west to east: Awate (AW), Bozi (BZ), Dabei (DB), Keshen (KS), and Kela (KL)^{10,17}. In this study, the western KTB includes the AW, BZ and DB segments (Fig. 1c). Given the relatively small area of the Awate segment, for simplification of discussion it is included within the Bozi-Dabei segment. The KTB was influenced by multi-stage tectonic movement, and developed a series of fault systems and fault-fold-related rows of structural traps. These traps primarily consist of en-echelon fractures in plan view. Vertically, the tectonic patterns of the traps primarily comprise thrust imbricate structure, where fault blocks, fault anticlines, and burst structures are superimposed on each other^{18,19}.

The Kuqa Depression is composed of Mesozoic and Cenozoic strata (Fig. 1d). A total of five sets of source rocks were developed: the Upper Triassic Huangshanjie and Taliqike formations (T_3h and T_3t), the Lower Jurassic Yangxia Formation (J_1y), and the Middle Jurassic Kezilenuer and Qiakemake formations (J_2kz and J_2q)²⁰. Here, T_3h and J_2q are lacustrine source rocks, and the other source rocks are coaly source rocks²¹. The present maturity of the Triassic-Jurassic source rocks varies from mature to highly mature or even over-mature²². The main exploration target layers are the Cretaceous Bashijiqike (K_1bs)⁵. The Paleogene Kumugeliemu and Suweiyi formation ($E_{1-2}km$ and $E_{2-3}s$) and the Neogene Jidike Formation (N_1j) are primarily composed of halite and anhydrite, and form excellent regional seals for hydrocarbon accumulation and preservation, with a thickness of 200–400 m^{4,16,23}.

The Kuqa Depression has experienced three significant evolutionary stages: a foreland basin (Permian–Triassic), an extensional rift basin (Triassic–Jurassic) and a rejuvenated foreland basin (since Cenozoic)^{16,24}. The tectonic history of the western KTB had three main stages (Fig. 1d): the Late Yanshan period, the Early Himalayan period, and the Late Himalayan period²⁵. During the Early Himalayan period there was relatively weak tectonic activity, and thick halite-anhydrite layers ($E_{1-2}km$ and $E_{2-3}s$) were deposited. From the N_1j sedimentary period, tectonic activity in the study area gradually became intensified and thrust faults were developed, which resulted in variable degrees of erosion of the $E_{2-3}s$. During the late Himalayan period, corresponding to the deposition of the Neogene Kangcun and Kuqa formation (N_1k and N_2k) strata, tectonic activity was very intense. With increasing plasticity of the halite-anhydrite layer ($E_{1-2}km$), a series of imbricate faults were developed under the $E_{1-2}km$, with large folds affecting the $E_{1-2}km$ strata.

Various factors jointly influence the formation and evolution of petroleum systems in the western KTB. Multiple sets of source rocks, characterized by large thicknesses, wide distribution, high abundance of organic matter, and high maturity, provided sufficient hydrocarbon supply^{4,26,27}. Due to rapid sedimentation in the Neogene, source rocks reached peak maturity in the Late Kuqa (N_1k) period⁶. Faults and traps formed by tectonic compression connect the underlying source rock layers with the overlying reservoirs, providing effective migration pathways and excellent sites for the accumulation of hydrocarbons²⁸. The two sets of halite-anhydrite layers ($E_{1-2}km$ and $E_{2-3}s$) were distributed widely and have good capping ability, thus providing protection for

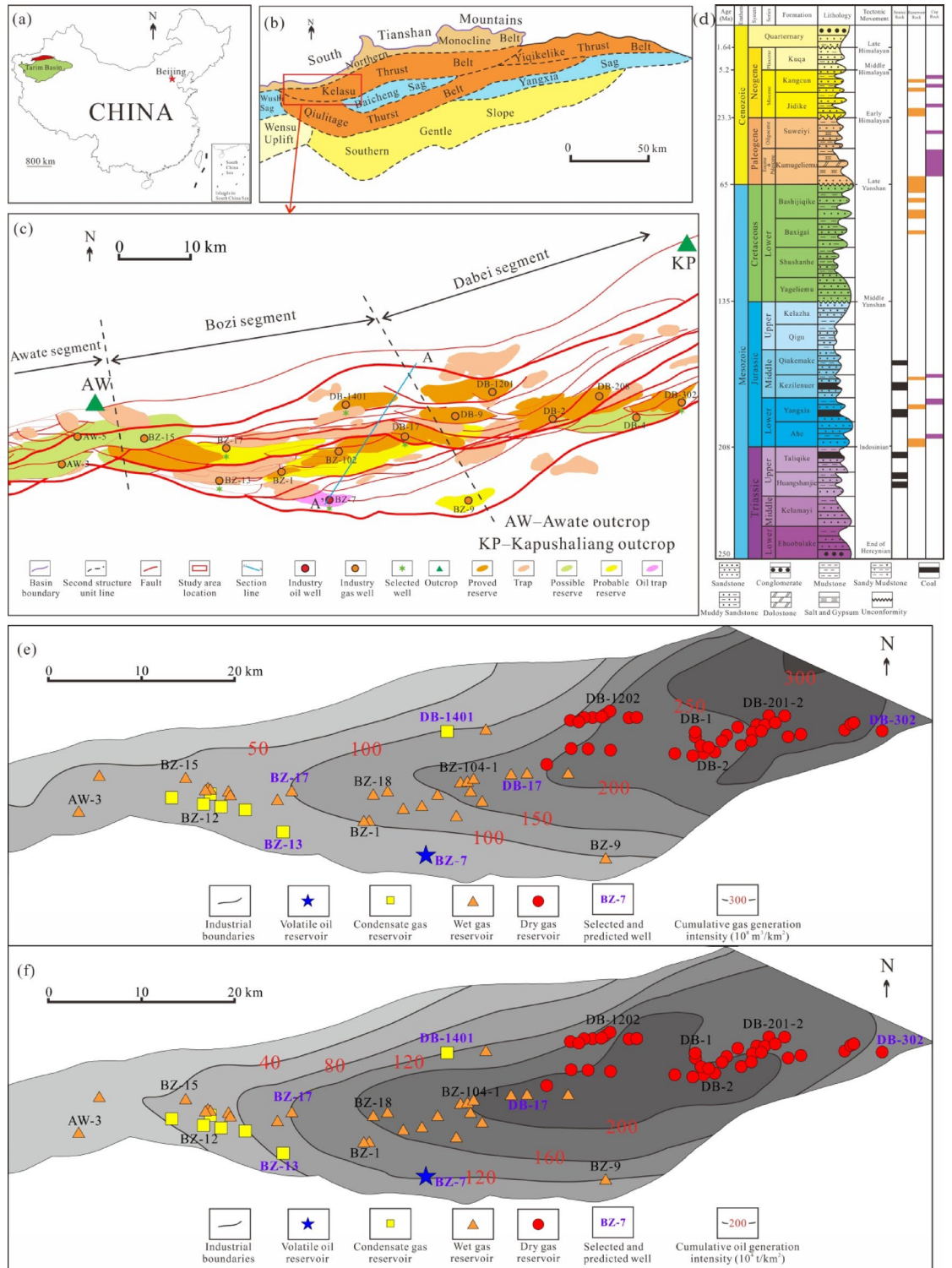


Fig. 1. Location and geology of the western Kelasu Thrust Belt in the Kuqa Depression, Tarim Basin. **(a)** Location map of the Tarim Basin and the Kuqa Depression in western China. **(b)** Distribution of the major structural belts and sags within the Kuqa Depression (modified from reference 7). **(c)** Division of three segments (Awate, Bozi, Dabei) and the distribution of wells, faults, and outcrops in the western Kelasu Thrust Belt. BZ = Bozi, DB = Dabei, AW = Awate. Green triangles show the outcrop locations. **(d)** Generalized Mesozoic-Cenozoic stratigraphic column of the Kuqa Depression (modified from reference 3), showing the key tectonic events and petroleum system elements, including the source rocks, multiple reservoir intervals, and cap rocks. **(e)** cumulative gas generation intensity of Triassic and Jurassic source rocks (modified from reference 8); **(f)** cumulative oil generation intensity of the Middle Jurassic Qiakemake Formation source rock (modified from reference 8).

oil and gas accumulation and preservation. The effective coupling of those geological conditions determines the distribution pattern of hydrocarbons in the western KTB, which exhibit the characteristics of multilayered compound hydrocarbon accumulations. It is generally accepted that the oil and gas charging process in the west KTB has the characteristics of oil first, gas later, and late transient accumulations^{28–30}.

Methods and data

To conduct a comprehensive analysis of the phase states and evolutionary characteristics in the western KTB, we selected six wells (BZ-7, BZ-13, DB-1401, BZ-17, DB-17 and DB-302) on the basis of the distribution of petroleum types spanning faults (Fig. 1c). These wells represent the four types of oil and gas discovered in the western KTB. We utilized fluid phase simulation to reconstruct the fluid phase states, and 1D basin modeling techniques to reconstruct geological evolution models. After combining their results of both, we assessed the evolutionary characteristics of the phase states and the fluid physics (density and viscosity).

Fluid phase simulation

The fluid phase simulation was conducted using PVTsim software developed by Calsep A/S, which establishes a fluid phase diagram after inputting detailed fluid information^{31–34}. The first step involved inputting fluid components (C_1 – C_{20+} and molecular weight) and other experimental data (constant mass expansion and constant volume depletion) derived from the PVT analysis reports provided by the Tarim Oilfield Company. The PVT analysis reports were compiled from updated fluid composition data obtained from wells after production conditions became stable. The software automatically selects the critical temperature, critical pressure, and other physical and chemical properties of each fluid component from the database. Subsequently, an appropriate fluid phase model was selected for simulation. In this case, we chose the Soave-Redlich-Kwong Equation of State³⁵. By inputting the required data or performing flash evaporation calculations under specific conditions, we obtained physical parameters such as phase envelope, gas-to-oil ratio (GOR), density, viscosity, etc. Based on the measured GOR, we repeatedly adjusted the gas fraction to achieve maximum consistency with the aforementioned physical parameters. The simulated fluid model can thus be considered a representation of the actual fluid in the reservoirs^{34,36,37}.

We inputted the initial fluid composition of six wells into the PVTsim software. After repeated calculations and tuning, the modeled physical parameters, including the density of the oil and gas and the GOR, matched as closely as possible with the measured physical parameters (Table 1). However, it is worth noting that there are certain discrepancies between the modeled and measured viscosity of oil, with the former consistently higher than the latter. This discrepancy can be attributed to multiple factors. The measured viscosity of oil is an average value and may deviate from the actual viscosity under conditions of 50 °C and 0.101 MPa. Additionally, the actual samples might be affected by non-hydrocarbon components or variable degrees of gas washing. Overall, the modeled results for selected wells are relatively accurate, and the restored fluid can be regarded as a useful model of an in-situ real fluid.

1D basin modeling

1D basin modeling is a powerful tool to reconstruct basin models and simulate the petroleum system by the evolution of thermal maturity, temperature, pressure, and hydrocarbon generation^{38,39}. In this study, we conducted 1D basin modeling using the Schlumberger PetroMod 2016 (1D) software. The main principles and procedures of basin modeling are detailed in previous studies^{34,36,39,40}. Three types of data are required for input into the software: stratigraphic parameters, including sedimentation ages, thickness, and lithology; tectonic events, including unconformities, erosion time, and erosion thickness; and boundary conditions, including heat flow, paleo water depth, and sediment water interface temperature.

Fluid Property		Gas			Oil			GOR	
Well		Production (m ³ /d)	Density (g/cm ³)	Viscosity (cP)	Production (m ³ /d)	Density (g/cm ³)	Viscosity (cP)*	GOR (m ³ /m ³)**	GOR (kg/kg)
BZ-7 (7540–7624 m)	Measured	36,509	0.0009	nd***	91.9	0.79	1.48	397	0.43
	Modeled	nd	0.0010	0.0103	nd	0.80	1.97	397	0.50
BZ-13 (7177–7259.5 m)	Measured	211,686	0.0008	nd	83.9	0.80	1.10	2,253	2.52
	Modeled	nd	0.0008	0.0108	nd	0.80	2.51	2,540	2.54
DB-1401 (6317–6555 m)	Measured	121,106	0.0009	nd	37.5	0.79	1.00	3,229	3.53
	Modeled	nd	0.0008	0.0109	nd	0.78	2.28	3,240	3.19
BZ-17 (6055.5–6088 m)	Measured	350,100	0.0008	nd	66.9	0.78	0.98	5,233	5.58
	Modeled	nd	0.0007	0.0110	nd	0.77	2.06	5,232	5.05
DB-17 (6058–6197.5 m)	Measured	318,009	nd	nd	11.2	0.81	1.07	28,394	24.63
	Modeled	nd	0.0007	0.0110	nd	0.80	2.38	28,408	25.27
DB-302 (7209–7244 m)	Measured	786,582	0.0008	nd	nd	nd	2.09	nd	nd
	Modeled	nd	0.0007	0.0111	nd	nd	nd	nd	nd

Table 1. Comparison of the measured and modeled physical parameters for wells BZ-7, BZ-13, DB-1401, BZ-17, DB-17 and DB-302. *The viscosity of oil was calculated under the conditions of 50 °C and 0.101 MPa. The measured value of viscosity is an average value. **Production GOR. ***nd = no data.

In this study, we obtained the stratigraphic parameters of the six wells from the completion reports supplied by the Tarim Oilfield Company. The tectonic history of the western KTB resulted in the appearance of unconformity interfaces at the Cretaceous Bashijiqike Formation/the Paleogene Kumugeliemu Formation, the Paleogene Suweiyi Formation/the Neogene Jidike Formation, and the Neogene Kuqa Formation/the Quarternary ($K_1bs/E_{1-2}km, E_{2-3}s/N_1j$ and N_2k/Q) (Fig. 1d). We collected the erosion time and thickness of each tectonic event from previous studies^{41–44}. The heat flow was relatively high in the Mesozoic (50–55 mW/m²), and decreased slowly but continuously during the Cenozoic, and decreased rapidly since 2 Ma, eventually reaching today's heat flow of 40–50 mW/m²^{45–47}. We estimated the paleo-water depth based on the sedimentary facies of each lithology^{48–50}. The sediment water interface temperature was selected automatically by inputting the region and latitude of each well in PetroMod 2016.

The evolution of phase States and features

Changes in reservoir temperature and pressure may influence phase state characteristics and evolution^{34,39}. Based on the assumption that a reservoir was formed without any destruction and change, and that the composition of the reservoir fluid was constant throughout the entire geological history, we derived the modeled reservoir temperature-pressure values (labeled as the reservoir P-T evolution line) from the PetroMod software at each time point of the entire geological history. We then overlay these on the phase diagrams, aiming to study the evolution characteristics of the phase states. The changes in temperature and pressure also affected fluid density and viscosity³⁶. We studied the evolutionary history of these by integrating the simulated fluid density and viscosity under the corresponding temperature and pressure at each time point over critical geological events.

Results

Restored fluid composition and fluid phase diagram

The real in-situ fluids were successfully simulated; the restored fluid compositions from the six wells are listed in Table 2. The simulated P-T phase diagrams for the fluids in the Cretaceous Bashijiqike Formation (K_1bs) are shown in Fig. 2. The fluid phase envelopes show the critical temperature (T_c), the critical pressure (P_c), the cricondetherm (T_m ; the maximum temperature at which liquids and vapor can coexist), and the cricondenbar (P_m ; the highest pressure at which a gas can exist in equilibrium with a liquid at a given temperature); and some (wells BZ-7 and DB-302) show the critical point (CP)³⁴. The values of T_c , P_c , T_m , and P_m of the fluid phase envelopes are depicted in detail in Fig. 2. On the whole, from well BZ-7 to DB-302, the T_m gradually decreases, while the P_m gradually increases and then rapidly decrease. Additionally, the areas of the fluid phase envelopes gradually increase, and then rapidly decrease (Fig. 2).

Well	Chemical compositions											
	N ₂	CO ₂	C ₁	C ₂	C ₃	iC ₄	nC ₄	iC ₅	nC ₅	nC ₆	nC ₇	nC ₈
BZ-7 (7540–7624 m)	1.28	0.30	52	9.6	4.4	1.05	1.8	1.06	1.13	2.3	9.3	4.7
	nC ₉	nC ₁₀	nC ₁₁	nC ₁₂	nC ₁₃	nC ₁₄	nC ₁₅	nC ₁₆	nC ₁₇	nC ₁₈	nC ₁₉	nC ₂₀₊
	2.8	2.0	1.18	0.95	0.75	0.71	0.57	0.43	0.38	0.30	0.26	1.10
BZ-13 (7177–7259.5 m)	1.11	0.38	80	8.7	2.6	0.51	0.53	0.20	0.13	0.12	0.32	1.23
	nC ₉	nC ₁₀	nC ₁₁	nC ₁₂	nC ₁₃	nC ₁₄	nC ₁₅	nC ₁₆	nC ₁₇	nC ₁₈	nC ₁₉	nC ₂₀₊
	1.27	0.82	0.52	0.31	0.22	0.17	0.13	0.10	0.067	0.057	0.044	0.20
DB-1401 (6317–6555 m)	2.2	0.22	85	5.6	1.41	0.35	0.41	0.13	0.11	0.19	0.65	0.76
	nC ₉	nC ₁₀	nC ₁₁	nC ₁₂	nC ₁₃	nC ₁₄	nC ₁₅	nC ₁₆	nC ₁₇	nC ₁₈	nC ₁₉	nC ₂₀₊
	0.44	0.39	0.31	0.25	0.20	0.22	0.15	0.11	0.098	0.078	0.065	0.31
BZ-17 (6055.5–6088 m)	1.7	0.39	88	5.8	1.25	0.24	0.27	0.12	0.079	0.060	0.10	0.19
	nC ₉	nC ₁₀	nC ₁₁	nC ₁₂	nC ₁₃	nC ₁₄	nC ₁₅	nC ₁₆	nC ₁₇	nC ₁₈	nC ₁₉	nC ₂₀₊
	0.22	0.26	0.19	0.16	0.19	0.12	0.11	0.078	0.065	0.056	0.050	0.28
DB-17 (6058–6197.5 m)	0.70	0.21	93	3.7	0.74	0.14	0.18	0.071	0.050	0.13	0.077	0.094
	nC ₉	nC ₁₀	nC ₁₁	nC ₁₂	nC ₁₃	nC ₁₄	nC ₁₅	nC ₁₆	nC ₁₇	nC ₁₈	nC ₁₉	nC ₂₀₊
	0.064	0.057	0.049	0.048	0.036	0.038	0.025	0.017	0.015	0.012	0.010	0.042
DB-302 (7209–7244 m)	0.55	0.78	97	1.23	0.16	0.033	0.032	0.014	0.007	0.014	0.006	0.018
	nC ₉	nC ₁₀	nC ₁₁	nC ₁₂	nC ₁₃	nC ₁₄	nC ₁₅	nC ₁₆	nC ₁₇	nC ₁₈	nC ₁₉	nC ₂₀₊
	nd*	nd	nd	nd	nd	nd	nd	nd	nd	nd	nd	nd

Table 2. The chemical compositions (N₂, CO₂ and C₁–C₂₀₊; mol %) of the restored fluids from wells BZ-7, BZ-13, DB-1401, BZ-17, DB-17 and DB-302. *nd = no data.

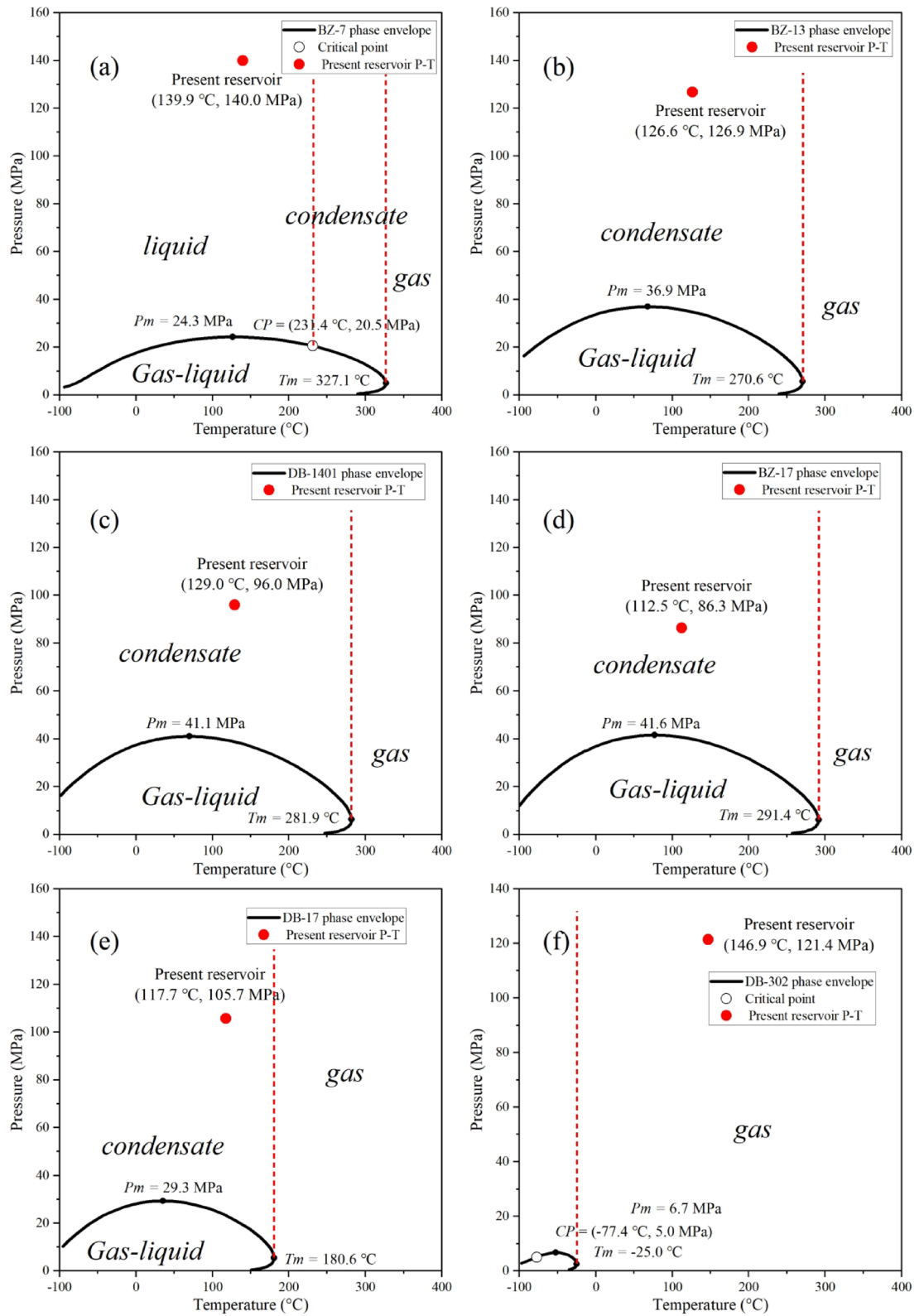


Fig. 2. The simulated P-T phase diagrams of wells (a) BZ-7, (b) BZ-13, (c) DB-1401, (d) BZ-17, (e) DB-17 and (f) DB-302. CP= the critical point, T_m = the cricondentherm, P_m = the criconobar.

According to the relative positional order of CP , T_m and P_m , the P-T phase diagram is divided into the gas-liquid coexistence phase zone, the liquid phase zone, the condensate phase zone, and the gas phase zone³⁴. By combining the distribution of the phase zone and the in-situ reservoir conditions, the fluids in the reservoir can be classified into various phases in the P-T phase diagrams. The reservoir fluid in well BZ-7 under in-situ reservoir conditions (139.9 °C, 140.0 MPa) was classified as a liquid phase (Fig. 2a). The reservoir fluids from wells BZ-13 and DB-1401 under in-situ reservoir conditions (126.6 °C, 126.9 MPa and 129.0 °C, 96.0 MPa, respectively) were classified as condensate phases (Fig. 2b, c). Theoretically, the reservoir fluids from wells BZ-17 and DB-17 under in-situ reservoir conditions (112.5 °C, 86.3 MPa and 117.7 °C, 105.7 MPa, respectively) were classified as condensate phases (Fig. 2d and e). Nevertheless, the production gas-oil ratios of wells BZ-17 (5,233 m³/m³ and DB-17 (28,394 m³/m³; Table 1) are higher than the threshold (3,562 m³/m³) between the condensate phase and the wet gas phase, and the gas dryness coefficient (C_1/C_{1-5}) of BZ-17 (92%) and DB-17 (95%) are lower than the threshold (95%) between the wet gas phase and the dry gas phase⁸. Thus, the reservoir fluids from wells BZ-17 and DB-17 under in-situ reservoir condition were re-classified into condensate (wet gas) phases. The reservoir fluid from well DB-302 has a gas dryness coefficient of 99% under in-situ reservoir condition (146.9 °C, 121.4 MPa), and was classified into the gas phase (Fig. 2f).

Based on the fluid composition, we can discriminate the type of phase state through several empirical statistical methods⁵¹⁻⁵³. The restored fluid composition data can be plotted on a ternary hydrocarbon phase state identification diagram of $C_1 + N_2$, $C_2-C_6 + CO_2$, and C_{7+} (Fig. 3a). This diagram shows that for most wells the fluid phase states in the reservoirs are condensate gas phase, except for the fluid in well BZ-7 which is a volatile oil phase. The C_{5+} versus C_1/C_{5+} discrimination diagram (Fig. 3b) shows that the fluids in wells BZ-7, BZ-13, DB-1401 and BZ-17 are condensate gas reservoirs with an oil ring, while the fluids in wells DB-17 and DB-302 are condensate gas reservoirs without an oil ring. The block fluid phase state identification diagram uses the proportions of C_1 to C_4 to discriminate fluid phase (Fig. 3c). Based on this diagram, well BZ-7 is an oil reservoir with a condensate gas cap, well BZ-13 is a condensate gas reservoir with an oil ring, wells DB-1401, BZ-17 and DB-17 are condensate gas reservoirs without an oil ring, and well DB-302 is a gas reservoir (Fig. 3c). Integrating

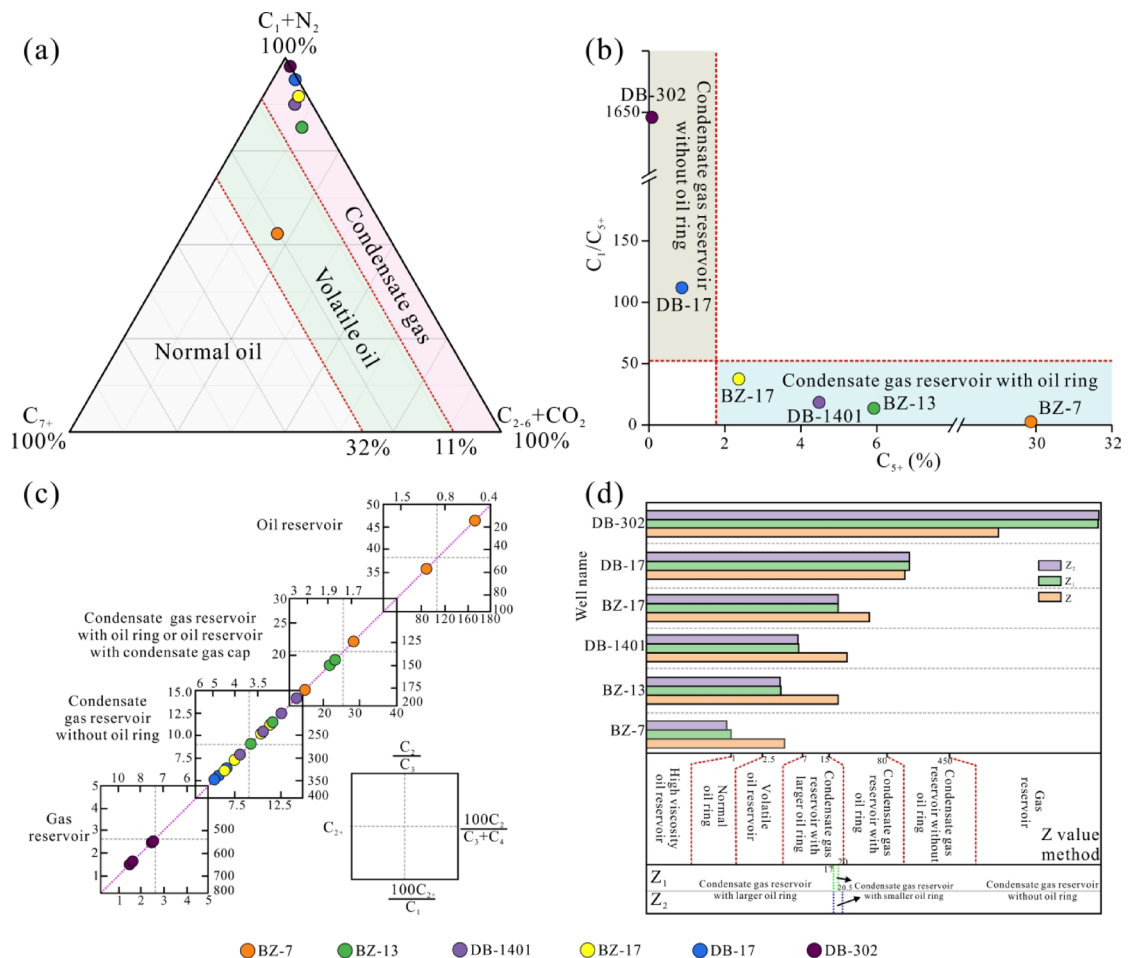


Fig. 3. Phase identification diagrams. (a) Ternary fluid component discrimination diagram, using $C_1 + N_2$, $C_2-C_6 + CO_2$, and C_{7+} . (b) C_{5+} versus C_1/C_{5+} discrimination diagram. (c) Block discrimination diagram, and (d) Z value discrimination and Z_1 - Z_2 factor discrimination. $Z = (C_1 + C_2 + C_3) / C_{5+} + C_2 / C_3$; $Z_1 = (0.88 \times C_{5+} + 0.99 \times C_1 / C_{5+} + 0.97 \times C_2 / C_3 + 0.99 \times F) / C_{5+}$; $Z_2 = (0.88 \times C_{5+} + 0.99 \times C_1 / C_{5+} + 0.97 \times C_2 / C_3 + 0.99 \times F) / C_{5+}$, where $F = (C_2 + C_3 + C_4) / C_{5+}$.

the Z value and Z_1 - Z_2 factor (Sun, 1996; Wang et al., 2024), well BZ-7 is a volatile oil reservoir, wells BZ-13 and DB-1401 are condensate gas reservoirs with a large oil ring, well BZ-17 is a condensate gas reservoir with a small oil ring, well DB-17 is a condensate gas reservoir without an oil ring, and well DB-302 is a gas reservoir (Fig. 3d).

Based on the analysis of P-T phase diagram (Fig. 2) and empirical statistical methods (Fig. 3), the reservoir types for well BZ-7 and DB-302 (dry gas reservoir) were conclusively classified into volatile oil and dry gas reservoirs, respectively. However, there seems a contradiction regarding the presence of oil rings in other reservoirs. Taking well DB-1401 as an example, it is identified as a condensate gas reservoir without an oil ring based on phase diagram analysis (Figs. 2b and 3c), while empirical statistical methods (Fig. 3b, d) conversely characterized it as containing an oil ring. This difference is caused by two key factors. First, the existing empirical methods rely primarily on fluid composition data with limited consideration of geological factors such as temperature and pressure conditions. Second, the phase behaviour of hydrocarbon is fundamentally governed by the temperature-pressure evolution histories, suggesting that the oil ring may preferentially form under lower temperature-pressure conditions but disappear in higher conditions. The latter is based on the analysis of the P-T phase diagram considering reservoir conditions and is the focus of this study, which consider more geological factors and does not contradict with the assessment by empirical statistical methods. A detailed discussion of these mechanisms is presented in Sect. 5.2.

Temperature and pressure histories of different wells

The burial histories of the Cretaceous Bashijiqi Formation (K_1bs) in the six wells were derived from PetroMod software (Fig. 4). The modeled pore pressure and temperature adapt well to the measured results, indicating a high level of reliability for the temperature and pressure histories modeled by the PetroMod software (Fig. 4a). The burial history of the Bashijiqi Formation (K_1bs) was mainly influenced by the Late Yanshan and the entire Himalayan orogenies (Fig. 4b). The rate of burial accelerated after the Early Himalayan tectonic movement, and uplift and erosion of the strata was most intense during the Late Himalayan period.

The modeled temperature and pore pressure histories of the Bashijiqi Formation (K_1bs) in the six wells is shown in Fig. 5. The temperature history is closely related to the heat flow and burial history, while the pore pressure history directly reflects the burial process and lithological changes^{34,37}. Both temperature and pressure increase from the Cretaceous to the present, and after the Late Paleogene, the rate of increase in both significantly accelerated. Erosional events caused by tectonic uplift affected the well locations differently. The temperature and pressure of most wells declined three times to varying degrees (Fig. 6b–f), except for well BZ-7 in which they declined four times (Fig. 6a). The temperature and pressure of the reservoirs in the six wells increased or decreased with burial depth and erosion of the formation by the same amplitude before 5.2 Ma (the

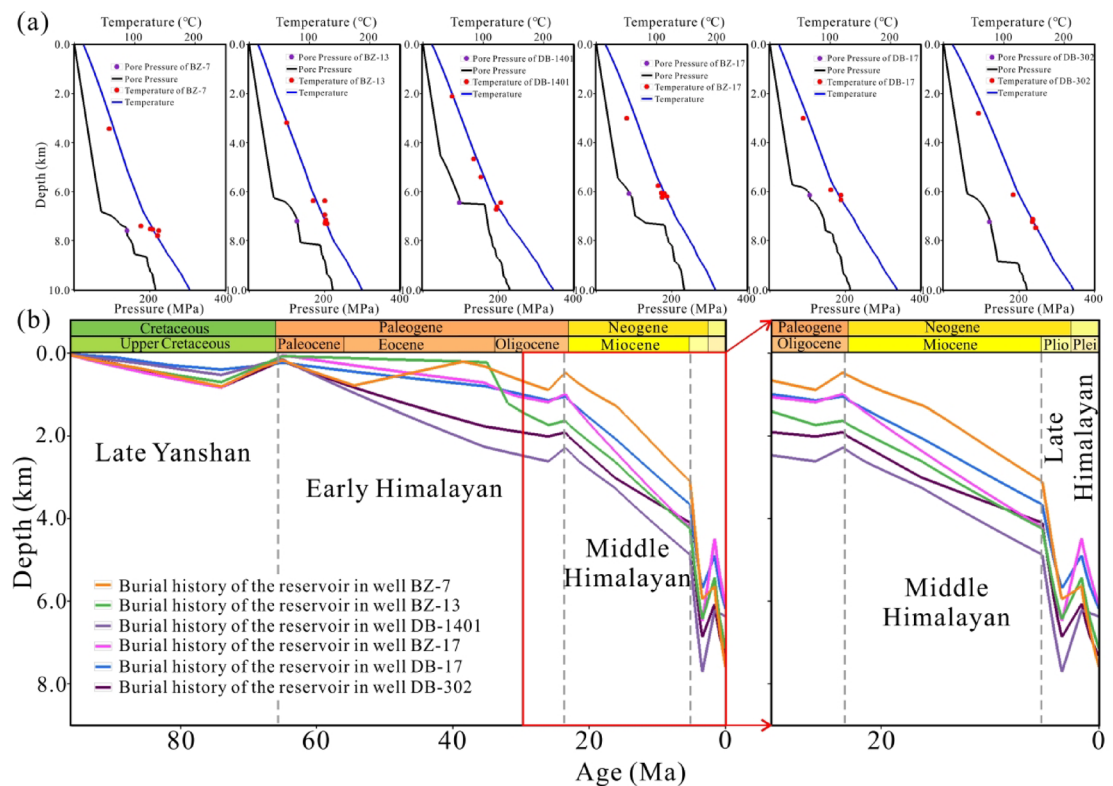


Fig. 4. Burial histories of the Lower Cretaceous Bashijiqi Formation (K_1bs) in the six wells. **(a)** The fits between the measured pore pressure and temperature and the modeled results for wells BZ-7, BZ-13, DB-1401, BZ-17, DB-17 and DB-302. **(b)** The burial history of the Bashijiqi Formation (K_1bs) in the six wells, showing that the rate of burial accelerated after the Early Himalayan orogeny. Plio = Pliocene, Plei = Pleistocene.

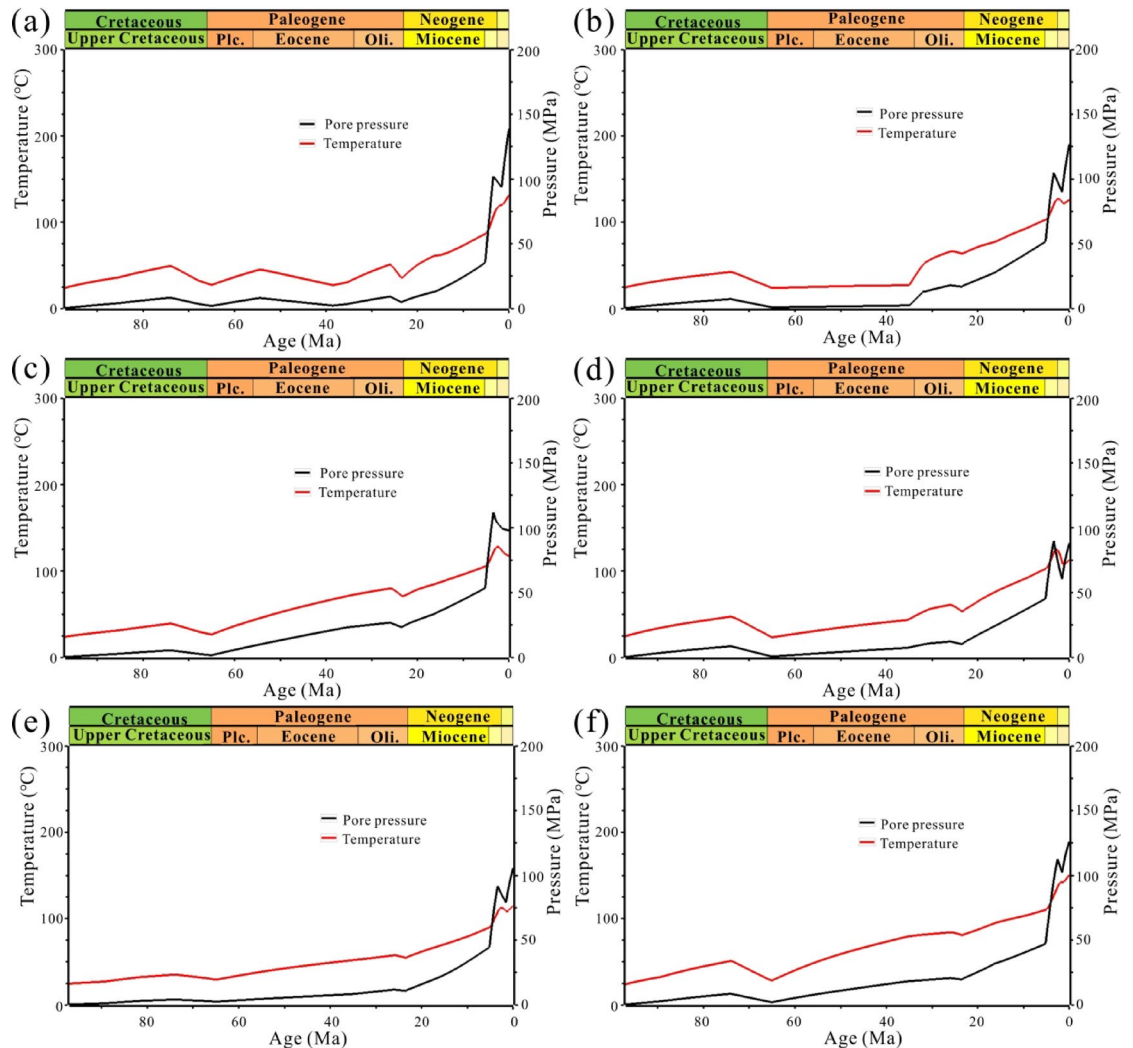


Fig. 5. Pore pressure and temperature histories of the Lower Cretaceous Bashijiqiike Formation (K_1bs) in wells (a) BZ-7, (b) BZ-13, (c) DB-1401, (d) BZ-17, (e) DB-17, and (f) DB-302. Plc = Paleocene, Oli = Oligocene.

Late Kangcun period). After 5.2 Ma in the Kuqa period, the change in pressure was significantly greater than the change in temperature, which may be due to a decrease in the paleo heat flow and thus a decrease in the geothermal gradient.

Characteristics of fluid phase evolution and physical properties (Density and Viscosity)

History of phase evolution

The phase envelope, along with the temperature and pressure evolution histories of the K_1bs reservoir, labeled as the reservoir P-T evolution line, were integrated to study the history of phase evolution (Fig. 6). The starting point of the reservoir temperature and pressure evolution is marked at 98 Ma, which corresponds to the time when the strata started to be deposited.

Significant phase differentiation processes are evident throughout the phase evolution histories of the six wells, except for well DB-302 (Fig. 6). For well BZ-7 (Fig. 6a), the reservoir P-T evolution line originates in the gas-liquid phase coexistence zone (GLPCZ) under the initial conditions (23.9 °C, 0.2 MPa). Despite the slow changes in the reservoir P-T evolution line due to the Late Yanshan (Cretaceous) and Early Himalayan (Paleogene) tectonic events, the phase remained within the GLPCZ. At 10.6 Ma during the Kangcun period, the reservoir P-T evolution line transitioned from the GLPCZ to the liquid phase zone at 71.5 °C and 23.1 MPa. Shortly thereafter, the reservoir P-T rapidly increased to 131.6 °C and 138.6 MPa, and remaining in the liquid phase zone until the present day, with a brief period of rapid decrease in P-T due to the Late Himalayan tectonic event.

For wells BZ-13 (Fig. 6b) and DB-1401 (Fig. 6c), the reservoir P-T evolution lines also started in the GLPCZ under initial conditions of 23.9 °C, 0.2 MPa and 23.9 °C, 0.2 MPa, respectively. Due to the Late Yanshan and Early Himalayan tectonic events, the reservoir P-T decreased slowly and then began to increase. At 12.1 Ma (BZ-13) and 12.2 Ma (DB-1401) in the Kangcun period, under conditions of 87.1 °C, 36.6 MPa and 92.2 °C, 40.7 MPa respectively, the reservoir P-T evolution line transitioned from the GLPCZ to the condensate phase

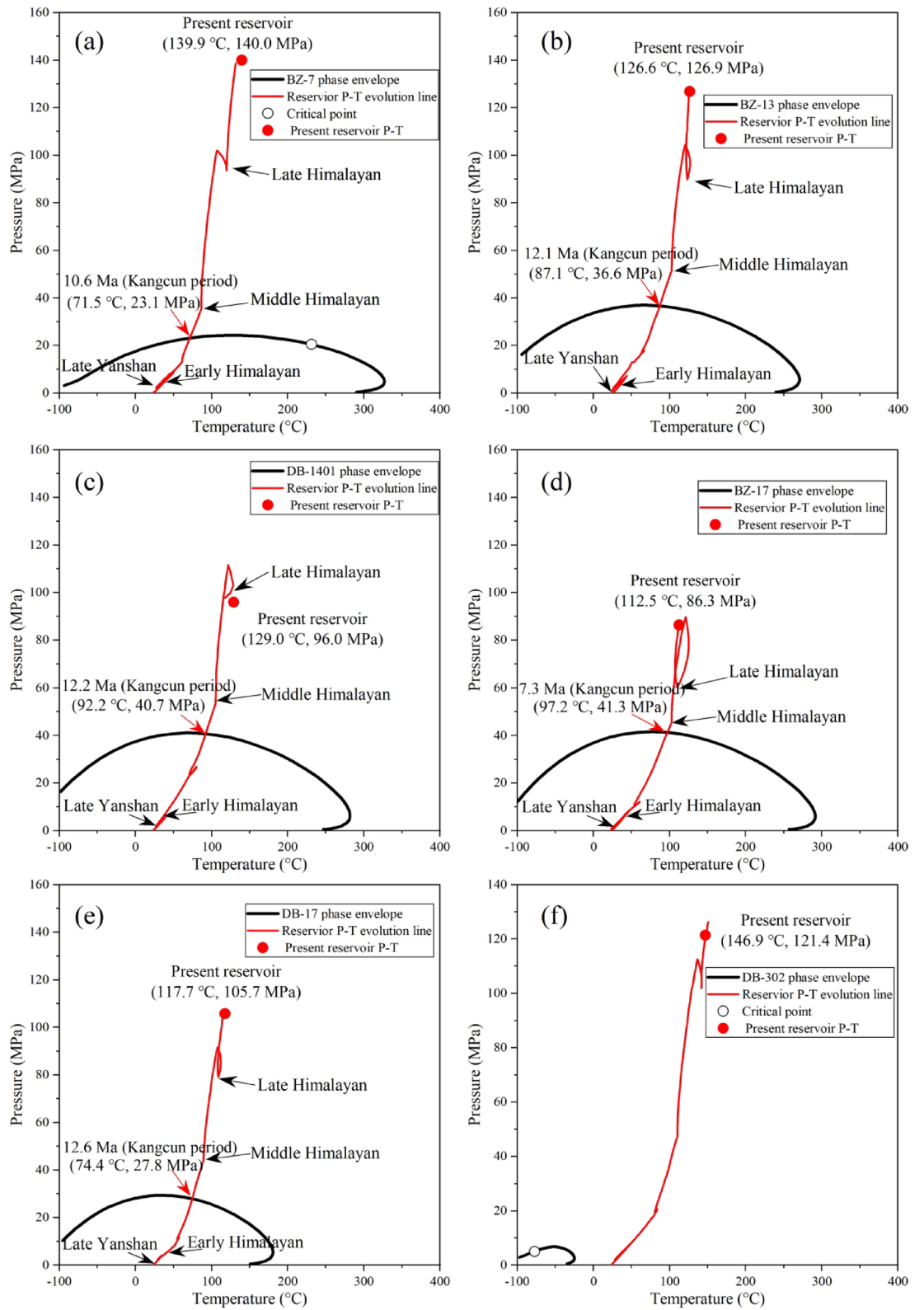


Fig. 6. The phase evolution history of the Lower Cretaceous Beshijiqike Formation (K_1bs) in wells (a) BZ-7, (b) BZ-13, (c) DB-1401, (d) BZ-17, (e) DB-17, and (f) DB-302.

zone. Following this transition, the reservoir P-T evolution line increased rapidly, with a brief period of rapid decrease due to the Late Himalayan tectonic event. The key difference between wells BZ-13 and DB-1401 lies in the trajectory of their reservoir P-T evolution lines post-Late Himalayan. The line for well BZ-13 decreased in P-T before increasing rapidly, whereas the line for well DB-1401 decreased in P-T and then remained constant. Ultimately, the reservoir P-T evolution lines for both wells remain in the condensate phase zone, under conditions of 125.5 °C, 127.0 MPa and 117.6 °C, 97.8 MPa, respectively.

For wells BZ-17 (Fig. 6d) and DB-17 (Fig. 6e), the reservoir P-T evolution lines began in the GLPCZ under initial conditions of 24.6 °C and 0.2 MPa. The reservoir P-T lines for these wells initially decreased slowly due to the Late Yanshan and Early Himalayan tectonic events, similar to wells BZ-7 and BZ-13, before rapidly increasing to 113.1 °C, 88.1 MPa and 115.1 °C, 105.7 MPa, respectively. These lines also experienced a brief period of rapid decrease in P-T due to the Late Himalayan tectonic event, but ultimately remained in the condensate (wet gas) phase zone. The key difference between wells BZ-17 and well DB-17 is the timing of their transition from the GLPCZ to the condensate (wet gas) phase zone. For well BZ-17, this transition occurred at 7.3 Ma in the Kangcun period, corresponding to conditions of 97.2 °C and 41.3 MPa, while for well DB-17, it occurred at 12.6 Ma in the Kangcun period, corresponding to 74.4 °C and 27.8 MPa. For well DB-302, the reservoir P-T line remained in the gas phase zone throughout its entire geological history, increasing from 24.0 °C to 0.2 MPa to 150.8 °C and 126.3 MPa (Fig. 6f).

The phase differentiation for all wells except for DB-302 occurred between 7.3 Ma and 12.6 Ma, corresponding to the Kangcun period. This indicates that the reservoir P-T line remained in the GLPCZ for a prolonged period in these five wells, and that the Kangcun period was crucial for oil and gas charge and accumulation.

Characteristics of fluid physical property evolution

The characteristics of the physical properties (density and viscosity) of the reservoir fluids vary throughout the entire geological history under different temperature and pressure conditions. Using the PVT simulation technique, the physical properties of the fluids were calculated under specified temperature and pressure conditions. The evolution histories of density and viscosity of the reservoir fluids from the K_1bs reservoir for several wells throughout geological history are shown in Figs. 7 and 8. The density and viscosity of the condensate or gas exhibit fluctuations, but generally show a clear tendency to increase over the entire geological history, while the overall trends for the liquids is a decrease in these properties, although there is much more variability than for the condensate or gas.

Except for the gas density of well BZ-7 (Fig. 7a) which reached 0.22 g/cm³ and entered the liquid phase zone after phase differentiation at 10.6 Ma, the other wells have a gradual decreasing trend of condensate or gas density from wells BZ-13 to well DB-302. These values are 0.45 g/cm³ for well BZ-13 (Fig. 7b), 0.40 g/cm³ for well DB-1401 (Fig. 7c), 0.36 g/cm³ for well BZ-17 (Fig. 7d), 0.34 g/cm³ for well BZ-17 (Fig. 7e), and 0.32 g/cm³ for well DB-302 (Fig. 7f). The density of the liquids in the six wells have a trend of first decreasing, then increasing, and then decreasing again with geological time (Fig. 7). For example, the density of liquid in well BZ-7 (Fig. 7a) shows a trend of first decreasing, then increasing, then decreasing, and finally increasing to 0.65 g/cm³ after phase differentiation in 10.6 Ma, with the current density of the fluid the second highest of the study. The current density of liquid in well DB-17 (Fig. 7e) is the highest of these wells, and its fluctuation with geological time is the smallest, with density ranging from 0.80 g/cm³ to 0.66 g/cm³. The density of the liquids becomes greater and the fluctuations become larger from wells BZ-13 to DB-17, with their ranges of variation being 0.80–0.51 g/cm³ for well BZ-13, 0.78–0.53 g/cm³ for well DB-1401, 0.77–0.57 g/cm³ for well BZ-17, and 0.80–0.66 g/cm³ for well DB-17.

The variability of the viscosity of the condensate or gas between the wells is less than that of density, while the variability of the viscosity of the liquid is greater than that of the density (Fig. 8). The viscosity of the condensate or gas tends to first increase slightly with geological time, and subsequently increase rapidly. The viscosity of the gas phase in well BZ-7 fluctuates weakly before the phase transition point (10.6 Ma), with values between 0.011 and 0.026 cP (Fig. 8a). The fluctuations in the viscosity of the condensate or the gas phase in the other wells gradually decrease with geological time, with the ranges of variation being 0.011–0.094 cP for well BZ-13, 0.011–0.073 cP for well DB-1401, 0.011–0.053 cP for well BZ-17, 0.011–0.050 cP for well DB-17, and 0.011–0.048 cP for well DB-302. The viscosity of the liquid phase before the phase transition point first decreases rapidly with geological time, then increasing rapidly, and finally declines slowly (Fig. 8). Notably, there is a small increase in the viscosity of the liquid phase in well BZ-7 after the phase transition point, with the values changing from 0.15 cP to 0.53 cP (Fig. 8a). The fluctuations in the viscosity of the liquid phase are variable for the other five wells during geological history, with the ranges of variation being 2.32–0.12 cP for well BZ-13, 2.95–0.16 cP for well DB-1401, 2.62–0.29 cP for well BZ-17, and 2.68–0.55 cP for well DB-17.

Discussion

Three distinct evolution paths of fluid phase-physical properties and the main controlling factors

Based on modeling and reconstruction results (Figs. 6, 7 and 8), three distinct evolution paths of fluid phase-physical property were identified. These are the transition from a GLPCZ to a liquid phase (well BZ-7), the transition from a GLPCZ to a condensate phase (wells BZ-13, DB-1401, BZ-17, and DB-17), and continuous maintenance in the gas phase (well DB-302). These paths suggest that the fluid chemical composition, along with the reservoir's temperature and pressure, exert a crucial influence on the fluid phase state^{10,54,55}. In the western KTB, temperature and pressure are interconnected and jointly controlled by burial history and paleo heat flow, thereby affecting the evolution of the fluid phase states. Reservoir temperatures less than 150 °C and pressures higher than 80 MPa at present show middle-low temperature, overpressured conditions (Figs. 2 and 6), supporting the conclusion that the western KTB experienced "prolonged shallow burial and late-stage rapid

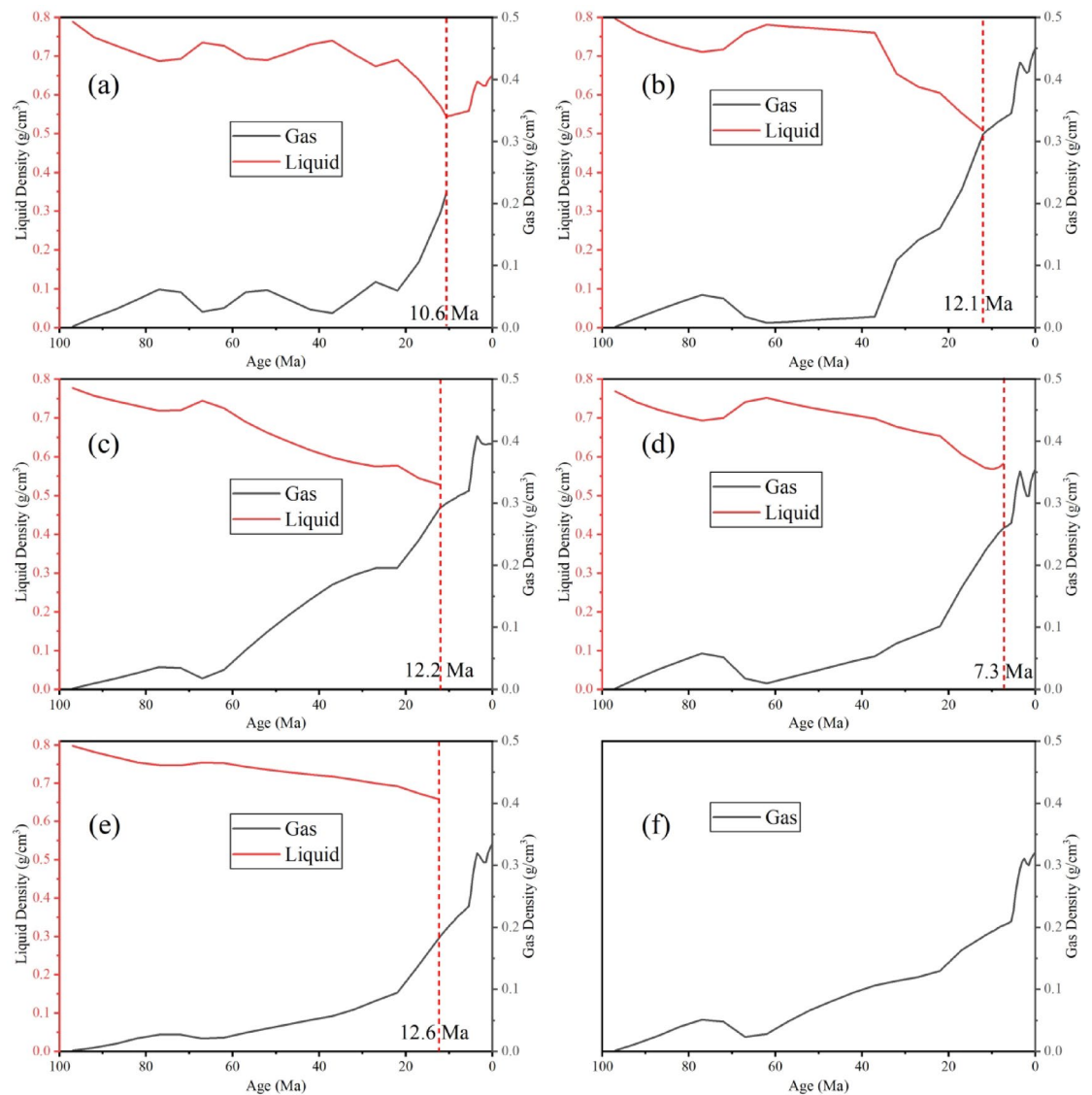


Fig. 7. The evolution histories of density of the gas and liquid fluids in the Lower Cretaceous Beshijiqike Formation (K_1bs) in wells (a) BZ-7, (b) BZ-13, (c) DB-1401, (d) BZ-17, (e) DB-17, and (f) DB-302. The red dashed line indicates the time of phase transition based on the reservoir P-T evolution lines (Fig. 6).

deep burial^{10,56}. The geological factors of low geothermal gradients, short heating duration and overpressures have postponed the increase of thermal maturity, which led to deepening of the oil window in the western KTB⁵⁷. Although the reservoir pressures have decreased rapidly due to the uplift caused by the Late Himalayan orogeny, the variations in reservoir pressures have not caused any significant changes in the phase states. Oils in the deep reservoirs have not been cracked due to the middle-low reservoir temperatures, resulting in the maintenance of single phase hydrocarbon accumulations, despite rapid burial.

Fluid redistribution and remigration, such as gas washing or gas mixing, may lead to changes in the composition of hydrocarbon fluids, thereby affecting their phase states. Based on previous studies about regional tectonic evolution and hydrocarbon generation history, the three different evolution models were summarized. The three different evolutionary paths mentioned above correspond to three distinct scenarios: (1) Early oil charge and no subsequent gas charge; (2) Early oil charge and subsequent gas charge; (3) Late gas charge with no or very small amount of early oil charge. The first scenario corresponds to well BZ-7, the third scenario corresponds to well DB-302, and the second scenario corresponds to the other four wells.

Fluid phase state characteristics and evolutionary patterns in the Western KTB

Based on the above discussion, the state of the liquid phases is influenced not only by the temperature and pressure in the reservoir but also by the accumulation stage. In this study, we further investigate the evolution of fluid phase states in the study area by combining the published hydrocarbon charging stages, basin modelling results, and phase simulation results. As shown in Fig. 9a, the source rock was shallowly buried over a long period of more than 200 Ma, followed by rapid burial over a short period of less than 30 Ma⁵⁹. Hydrocarbon

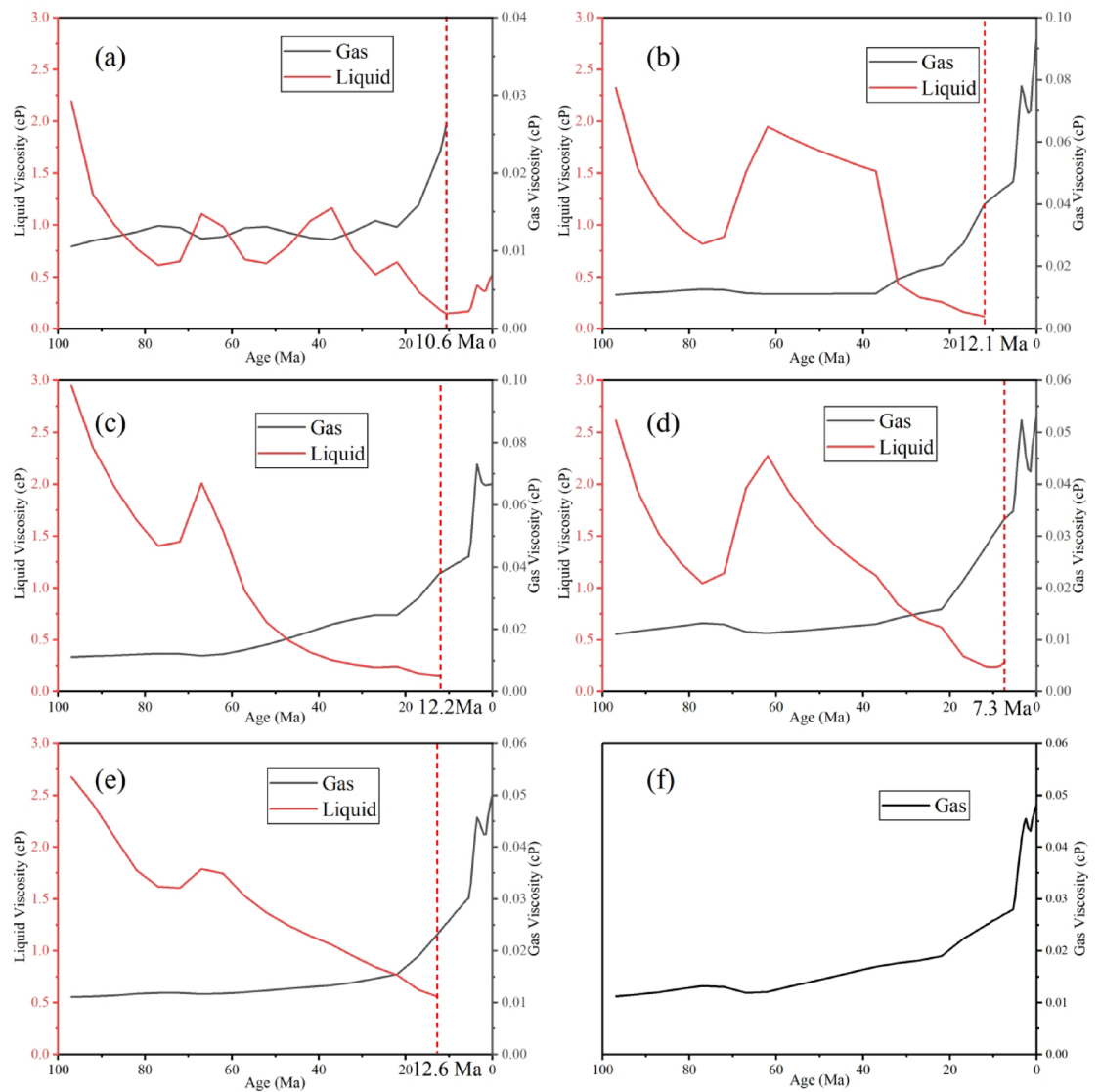


Fig. 8. The evolution histories of viscosity of the gas and liquid fluids in the Lower Cretaceous Beshijiqike Formation (K_1bs) in wells (a) BZ-7, (b) BZ-13, (c) DB-1401, (d) BZ-17, (e) DB-17, and (f) DB-302. The red dashed line indicates the time of phase transition based on the reservoir P-T evolution lines (Fig. 6).

generation in the study area occurred relatively late, beginning at the Neogene. The Triassic-Jurassic source rocks underwent sequential oil generation periods. The Triassic source rocks generated oil firstly, followed by the Jurassic source rocks, and subsequently entered a gas generation for both formations⁶⁰ (Fig. 9b).

The characteristics and evolutionary pattern of the fluid phase in western KTB are relevant to the history of hydrocarbon generation, the formation and evolution of traps, and accumulation processes. These aspects are influenced by the tectonic evolution of the Kuqa Depression, driven by the movement of South Tianshan Mountains. Previous researchers have suggested that hydrocarbon accumulation in this region typically follows an “early oil and late gas” pattern^{61–63}, which is closely tied to tectonic evolution. The Kuqa Depression has experienced three tectonic stages: a foreland basin, an extensional rift basin, and a rejuvenated foreland basin (Fig. 10). Of these, the rejuvenated foreland basin stage, commencing in the Late Cenozoic, is particularly significant. Major tectonic movement in the Bozi-Dabei area generally began after deposition of the Neogene Jidike Formation (N_1j), peaked during the deposition of the Neogene Kuqa Formation (N_2k), and continued to the present day¹⁰.

The first tectonic stage spans from the deposition of the Jidike Formation (N_1j) to the deposition of the Kangcun Formation (N_1k ; 16–5 Ma; Fig. 10a). During this period, the Triassic source rocks reached peak oil generation. However, minimal structural deformation occurred, and few faults were developed, indicating that traps in the western KTB had not yet formed²⁰. Due to the absence of effective migration conduits and traps, the early oil generated from the Triassic source rocks primarily migrated laterally from north to south along unconformity surfaces or within porous sandstone beds (Fig. 10a). Consequently, few oil reservoirs were formed in the Bozi segment during this stage. Despite this, there is evidence of reservoir bitumens, fluorescence,

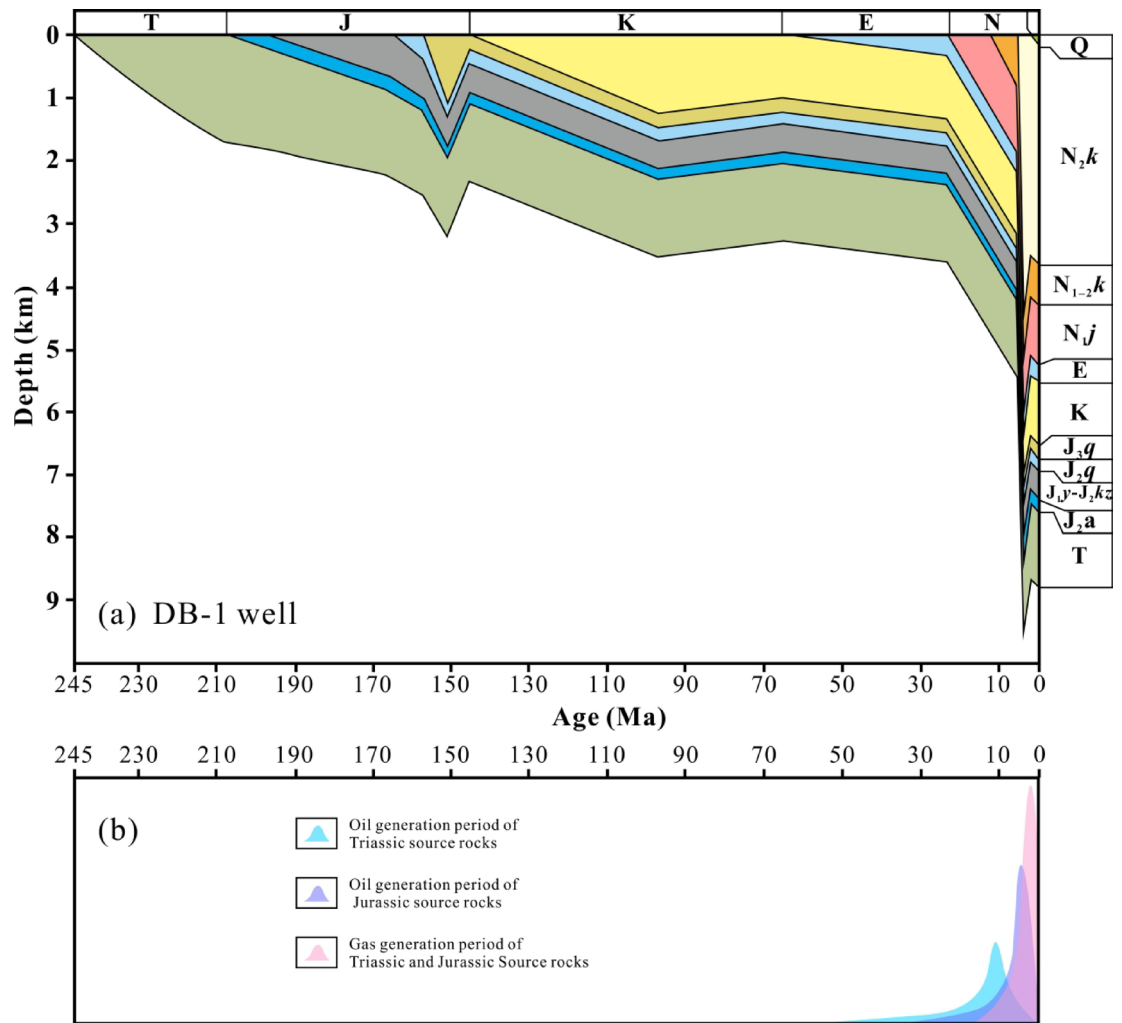


Fig. 9. Burial history and source rock hydrocarbon generation evolution history diagram. (a) Burial history of DB-1 well (modified from reference 59); (b) Evolution of hydrocarbon generation in Bozi segment (modified from reference 60).

and petroleum fluid inclusions, which suggest that early oil filling occurred in the Dabei sub-salt Bashijiqi Formation (K_1bs) reservoir⁶². In other words, some relatively suitable traps developed in the Dabei segment, allowing a portion of the early oil to migrate along faults and accumulate in these traps under the salt layer, forming the early Dabei sub-salt paleo oil reservoirs.

The second tectonic stage extends from deposition of the Kangcun Formation (N_1k) to the deposition of the Kuqa Formation (N_2k ; 5–3.4 Ma; Fig. 10b). With increasing maturity of the Jurassic and Triassic source rocks, large quantities of light oil and gas were generated (Fig. 10b). During this time, tectonic compression of the western KTB strengthened in a roughly south-north direction. Reverse faults, formed during the Mesozoic, were reactivated, and thick sediments from the piedmont area were rapidly deposited in the southern Baicheng Sag of the Kelasu area, leading to the development of a small number of traps¹⁰. Light oil and gas migrated along these faults, significantly contributing to the formation of the current oil reservoirs in the western KTB, such as in well BZ-7⁶⁰. However, the early Dabei sub-salt paleo-oil reservoirs were destroyed by salt-penetrating faults, causing loss of the light oil and gas derived from the Jurassic source rock, along with loss of a portion of the high maturity light oil generated from the deep Triassic source rocks. Therefore, oil and gas migrated upwards along faults and converges again in shallow traps, forming residual oil reservoirs^{28,61}.

The third tectonic stage started during the deposition of the Kuqa Formation (N_2k) and continued to the present (3.4–0 Ma; Fig. 10c). During this period, intense tectonic movement and deposition of thick Quaternary sediments led to the rapid development of more thrust faults and folds beneath the salt layer, resulting in the formation of more traps. Rapid subsidence resulted in the Triassic source rocks becoming high and even over-mature in a short time, and they entered the stage of dry gas generation. Very deep burial and intense tectonic compression resulted in plastic deformation of the salt layer and the extinction of faults in the salt-interbed, forcing fault closures^{28,64}. As a result, the dry gas accumulated only beneath the salt layer, rather than migrating upwards along the faults. As further illustrated in Fig. 1e, the gas generation center of the Triassic and Jurassic source rocks is in the northeastern part of the study area^{6,8}. The dry gas migrated upward through fault systems

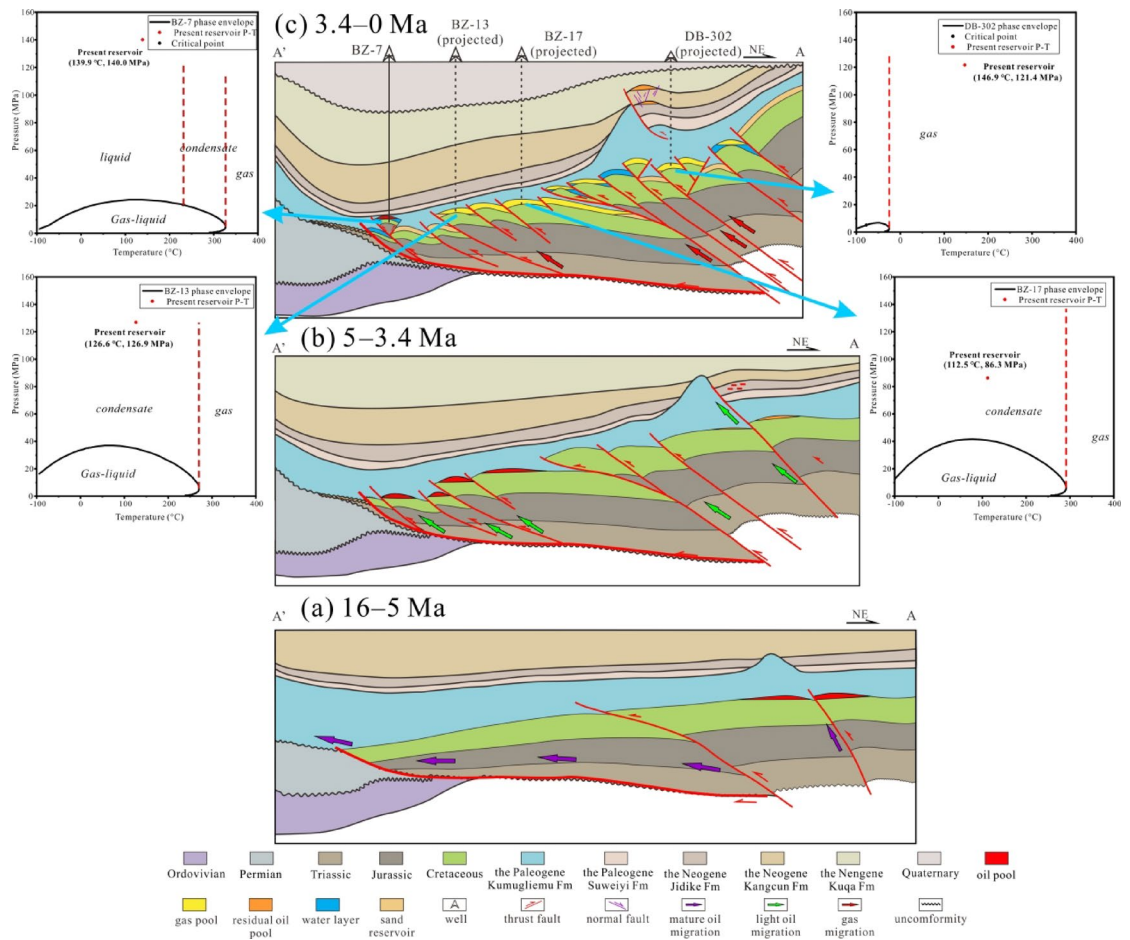


Fig. 10. Cross sections showing the evolution of hydrocarbon charges in the Bozi-Dabei area of the Kuqa Depression, Tarim Basin in three time slices. (a) Depositional period of the Kangcun Formation from 16–5 Ma; (b) Depositional period of the Kuqa Formation from 5–3.4 Ma; (c) Depositional period of the Quaternary from 3.4–0 Ma. Fm = Formation. The four simulated P-T phase diagrams are simplified from Fig. 2, and show the connection between hydrocarbon charge history and the P-T evolution of the four wells. The position of the cross section A–A' is shown on Fig. 1c. The black dashed lines represent the projected wells.

along a general northeast-to-southwest direction, leading to a subsequent large-scale injection of dry gas that caused intense gas washing effects in the early-formed oil reservoirs.

The Dabei segment is near the hydrocarbon generation center, hence the amount of dry gas charge gradually decreased from the Dabei segment to the Bozi segment. As shown in the Fig. 1e, the cumulative gas generation intensity ranges from 200×10^8 to 300×10^8 m^3/km^2 within the Dabei segment and from 50×10^8 to 150×10^8 m^3/km^2 within the Bozi segment. This means that the residual sub-salt oil reservoirs in the Dabei segment were subjected to more intense gas washing or gas mixing, with a pattern of increasing GOR from the southwest to the northeast (Fig. 1c). For instance, the GOR of well BZ-7 is $397 \text{ m}^3/\text{m}^3$, well BZ-102 is $9,170 \text{ m}^3/\text{m}^3$, well DB-17 is $28,394 \text{ m}^3/\text{m}^3$, well DB-9 is $308,195 \text{ m}^3/\text{m}^3$, and well DB-1201 is $504,948 \text{ m}^3/\text{m}^3$ ⁸. This also led to the rough distribution of the fluid phase state, with gas phase fluids in the inner ring, condensate phase fluids in the middle ring, and liquid phase fluids in the outer ring. Simultaneously, the large quantities of gases generated from the Triassic-Jurassic source rocks enhance the possibility of an alternative mechanism for condensate formation. This namely condensation mechanism involves oil and gas accumulations resulting from phase separation of upward hydrocarbon flow^{58,65}. The amount of upward hydrocarbon flow may decrease with increasing migration distance, as well as the distance from the kitchen to the traps, to help fully understand the whole process of hydrocarbon accumulations around thrust-belts.

Phase differentiation occurred at 7.3–12.6 Ma (corresponding to the deposition of the Kangcun Formation, N_1k) for all wells except for DB-302 (Fig. 6), suggesting that oil and gas charging occurred during the Kangcun period. Based on the discussion above, we assume that the chemical compositions of the fluid in well BZ-7 remained constant after accumulation, while that of the other wells were changed by varying degrees of gas washing. The phase states of the other wells were transformed from GLCP to the liquid phase and then to the condensate phase, and finally to the gas phase. Based on taking the fluid composition of well BZ-7 as the initial fluid compositions for the other wells, the evolution of the density of fluids in the Bashijiqike Formation (K_1bs) are presented in Fig. 11.

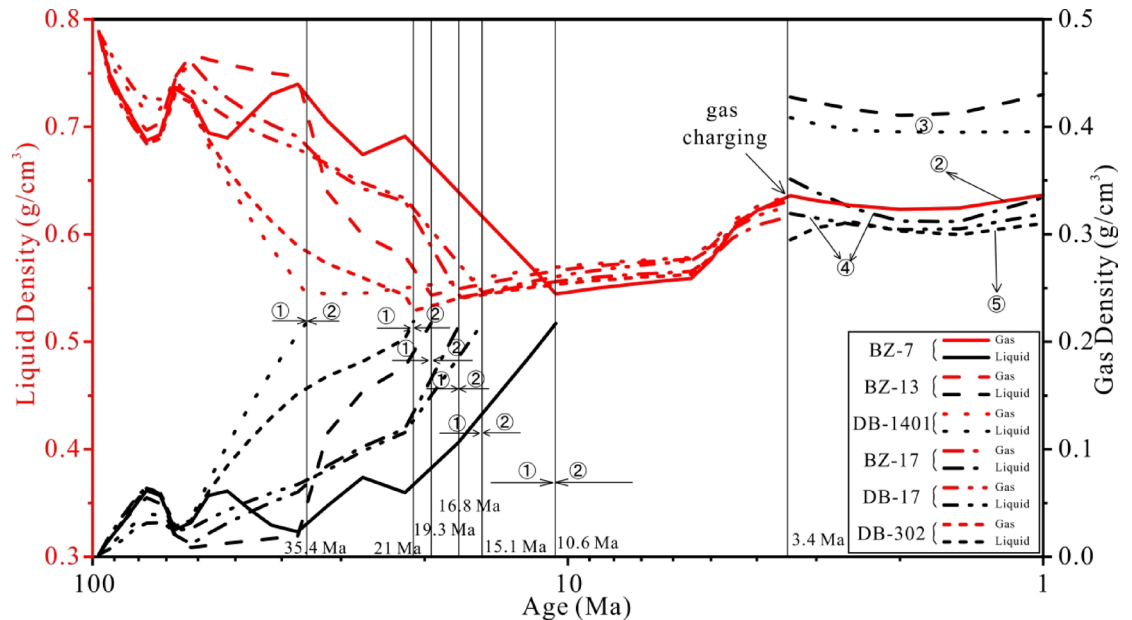


Fig. 11. The evolution of the fluid density in the Lower Cretaceous Beshijiqike Formation (K_1bs) in the six wells, taking the chemical composition of the well BZ-7 as the initial chemical compositions for the other wells. The red lines show the liquid density, and the black lines show the gas density. ①: the gas-liquid coexistence phase; ②: the liquid phase; ③: the condensate phase; ④: the condensate (wet gas) phase; ⑤: the dry gas phase.

The fluids transformed from the GLCP to the liquid phase at different time points: BZ-7 at 10.6 Ma, BZ-13 at 19.3 Ma, DB-1401 at 35.4 Ma, BZ-17 at 16.8 Ma, DB-17 at 15.1 Ma, and DB-302 at 21 Ma (Fig. 11). Those time points concentrate on 10.6 Ma–21 Ma, corresponding to the deposition period of Early Neogene (from N_1j to N_1k). During this interval, the Triassic source rocks reached the main oil-generation stage^{5,26}. It suggests that two-phase hydrocarbon accumulations may have formed by this time at relatively shallower positions, potentially explaining the contradiction regarding the oil ring mentioned above. With increasing burial depth, the phase states consistently remained as the liquid phase until the Late Kuqa period (3.4 Ma). After 3.4 Ma, large amounts of dry gas migrated into the early oil reservoirs, leading to varying degrees of gas washing. Due to “forward spreading” faults (faults formed from the hinterland to the front) and the location of the main hydrocarbon generation kitchen, the gas charging time, intensity and amount in the Dabei segment were earlier and greater than that in the Bozi segment. As shown in Fig. 1f, the center of oil generation intensity within study area is biased to the Dabei segment with values exceeding 160×10^4 t/km², which contrasts with the Bozi segment with values between 40×10^4 and 200×10^4 t/km², 120×10^4 t/km² on average. Conversely, the cumulative gas generation intensity in the Dabei segment ranging from 200×10^8 to 300×10^8 m³/km² is much higher than that in the Bozi segment ranging from 50×10^8 to 150×10^8 m³/km². Even if there were early oil reservoirs in the Dabei segment, large amounts of dry gas were charged into those reservoirs, resulting in very high GORs. Little dry gas was charged into the early oil reservoirs in the Bozi segment, and the impact gradually weakens from north to south, with the intensity of gas charging and the amount of dry gas decreasing.

In conclusion, it is evident that the main factors that control phase states in the western KTB are the coincidence of the trap formation period with the main hydrocarbon generation period of the source rocks, and the communication between the faults and the hydrocarbon source kitchen. Oil and gas at different thermal evolution stages could be captured at different times and tectonic settings in the accumulation process⁵⁵. In addition, the distribution and thickness of source rocks, and difference in the parent material and thickness of the salt layer also probably influence the fluid phase state^{55,66}.

Examining the assumptions and implications of constant fluid composition in hydrocarbon phase evolution

Here, it must be emphasized that the above results, whether they concern the evolution of phase states or the physical properties of the fluid, are based on the assumption that the reservoir was formed without destruction or alteration and that the composition of the reservoir fluid has remained constant throughout the entire geological history. Notably, given the complex geological setting in the western KTB, characterized by multi-stage tectonic movements^{16,24}, plastic deformation of salt layers²⁸, faults activities, and rapid burial⁶⁷, it is challenging to directly quantify the variations of fluid composition throughout the geological history. The main purpose of this assumption is to consider the fluid composition within each reservoir as constant and thus investigate how temperature and pressure conditions act as the main controlling variables in shaping phase evolution in the thrust belt setting. By temporarily fixing the fluid composition, the direct impact of temperature and pressure changes on the pathways of phase differentiation can be more clearly decoupled. Similar solutions have been successfully used in previous studies of phase evolution^{34,36,37,68}, which have been fully proven effective.

However, secondary alteration like gas washing and mixing effects may lead to change in fluid compositions during geological processes^{69,70}, which was not considered in this assumption and also leads to some limitations. Despite these assumptions, the geological setting of the western KTB, characterized by prolonged shallow burial coupled with late-stage rapid deep burial and short-term oil and gas charging as shown in Fig. 9, provides applicability for this assumption. For example, even if the fluid composition from well BZ-7 is assumed to be the initial fluid composition with negligible secondary alterations for other wells, the timing of phase differentiation may occur between 15.1 and 21 Ma (the Early Neogene) (Fig. 11). This does not differ significantly from the previously determined time between 7.3 and 12.6 Ma, which corresponds to the Early Neogene (Fig. 6). This result suggests that the influence of fluid composition on phase evolution histories may coincide with the predominant duration of phase differentiation. This observation supports the applicability of the assumption in the western KTB context.

Additionally, we selected four different types of oil and gas reservoirs to represent variations that may have occurred during tectonic history. The different compositions of fluid are the results of different tectonic histories, and incorporating these fluids for comparison allows us to understand their evolution and changes. Within this confined petroleum system, one fluid type can transform into another through oil mixing and gas injection/washing processes. While we have not considered explicitly individual traps, our analysis encompasses the entire system which may contain all types of fluids associated with the staged history. This is the main objective of our research: to understand the whole from fragmented information. Nonetheless, future studies would benefit from integrating phase kinetics with tectonic evolution to quantify the combined influence of fluid composition and temperature and pressure evolution on phase evolution history. This is a research direction that is both necessary and promising.

Significance for understanding and guiding thrust fault-related exploration

Faults play a relatively complex role in the oil and gas accumulation process. On one hand, faults can be taken as efficient migration conduits, connecting deep source rocks and shallow reservoirs. Hydrocarbon can migrate upward, and accumulate to form oil and gas reservoirs. On the other hand, faults may also cause the readjustment of paleo oil or gas reservoirs, destroy the preservation conditions of oil and gas reservoirs, and make oil and gas accumulations subject to leakage, biodegradation, gas washing, water washing, oxidation, and other destructive effects⁷¹. Even so, the contribution of faults to oil and gas migration and accumulation is incomparable to other migration paths (e.g. unconformity surfaces, and permeable carrier beds). Tectonic history and the formation time of faults determine oil and gas distribution from a piedmont thrust belt to the interior of a basin⁷². It should be noted that the fault system in the western KTB is dominantly of forward extension^{12,73,74}. The piedmont thrust zone suffered strong tectonic deformation, and faulting resulted in the migration and loss of oil and gas. In contrast, with the propagation of deformation to the interior of a basin and the increasing burial depth of strata, the lateral plugging properties of faults is significantly enhanced, and an oil and gas distribution with different “stepped” structural belts can be formed.

Many recent reports have catalogued the occurrence of this tectonic control in the Tarim Basin^{56,75}. With progressively more deep and ultra-deep oil and gas exploration, it is necessary to correctly understand the evolution pattern of fluid phase states in thrust fault-related traps, in order to accurately predict the fluid phase states in deep reservoirs. This study also provides theoretical guidance for seeking favorable exploration areas, and increasing the reliability of petroleum development in compressional tectonic settings.

Conclusions

This paper highlights the need for quantitative reconstruction of phase states and evolution characteristics of oil and gas in compressional tectonic settings. Simulated P-T phase diagrams elucidate that present reservoir fluids for six wells in the western Kelasu Thrust Belt (KTB) in the Kuqa Depression, Tarim Basin, exist in different phases. These are the liquid phase (well BZ-7), the condensate phase (wells BZ-13 and DB-1401), the wet gas phase (wells BZ-17 and DB-17), and the dry gas phase (well DB-302). Modeled temperature and pressure histories show a slow increase in temperature and pressure before the Neogene, and then rapidly increase to the present day, corresponding to long-term shallow burial and late-stage rapid deep burial. Phase evolutionary histories show that the reservoir fluids experienced phase transformation in five of the wells, changing from the gas-liquid coexistence phase (GLCP) to the liquid phase or the condensate phase. There was continuous maintenance of the gas phase in well DB-302.

With some variabilities, the density and viscosity of the liquid phase gradually decreased with geological time, while that of the gas phase generally increased. In addition, the variation of density and viscosity of the oil and gas is associated with GORs and the types of oil-gas reservoir, and there is a tendency in the western KTB for a change from volatile oil reservoirs, to condensate reservoirs, to condensate (wet gas) reservoirs, to dry gas reservoirs.

Three different evolution pathways are presented, which represent three distinct scenarios: (1) Transition from GLCP to liquid phase, resulting from the reservoir formation mechanism by mainly early oil charge with no or minor late gas charge. (2) Transition from GLCP to condensate phase, resulting from the reservoir formation mechanism by early oil charge and subsequent gas charge. (3) Continuous maintenance in the gas phase, resulting from the reservoir formation mechanism by a large amount of late gas charge with no or very small amount of early oil charge. The change of both fluid composition and reservoir temperature and pressure may cause variation of the phase states. However, phase state evolution is more sensitive to the fluid composition than reservoir temperature and pressure under such geological setting of intense tectonics. It means that the fluid composition is the decisive factor to control phase states in the Bozi-Daebei area.

A pattern of “two early stages of oil-filling followed by a later gas-charging stage” is proposed, which suggests that the main factors that control phase states in the western KTB are the coincidence of the trap formation

period with the main hydrocarbon generation period of the source rocks, and the communication between the faults and the hydrocarbon source kitchen. During exploration in thrust fault-developed areas, correctly understanding the evolutionary characteristics of the phase state and physical properties of deep fluids is vital for predicting current fluid phase state. This not only provides theoretical guidance, but increases the reliability of further petroleum exploration and development in compressional tectonic settings.

Data availability

The datasets used and/or analysed during the current study available from the corresponding author on reasonable request.

Received: 3 January 2025; Accepted: 22 May 2025

Published online: 02 June 2025

References

- Huang, W. K. et al. Petroleum generation potentials and kinetics of coaly source rocks in the Kuqa depression of Tarim basin, Northwest China. *Org. Geochem.* **133**, 32–52. <https://doi.org/10.1016/j.orggeochem.2019.04.007> (2019).
- Chai, S., Li, C., Lu, X., Zhuo, Q. & Gong, Y. Geometry and kinematics of Tugerming structural belt in the East of Kuqa depression, Tarim basin. *Pet. Res.* **6**, 333–350. <https://doi.org/10.1016/j.ptlrs.2021.05.008> (2021).
- Guo, X. W. et al. Effects of tectonic compression on petroleum accumulation in the Kelasu thrust belt of the Kuqa Sub-basin, Tarim basin, NW China. *Org. Geochem.* **101**, 22–37. <https://doi.org/10.1016/j.orggeochem.2016.08.008> (2016).
- Jia, C. & Li, Q. Petroleum geology of Kela-2, the most productive gas field in China. *Mar. Petrol. Geol.* **25**, 335–343. <https://doi.org/10.1016/j.marpetgeo.2008.01.002> (2008).
- Yang, H. et al. Reservoir accumulation conditions and key exploration & development technologies for Keshen gas field in Tarim basin. *Pet. Res.* **4**, 295–313. <https://doi.org/10.1016/j.ptlrs.2019.09.004> (2019).
- Yang, X. et al. Formation mechanism of the Bozi-Dabei trillion cubic natural gas field, Kuqa foreland thrust belt. *Earth Sci. Front.* **29**, 175–187 (2022).
- Wang, K. et al. Characteristics and formation mechanism of lower cretaceous deep and ultra-deep reservoir in Bozi-Dabei area, Kuqa depression. *J. China Univ. Min. Technol.* **51**, 311–328 (2022).
- Mo, T. et al. The phase characteristics and controlling factors of oil and gas in the West of Kelasu structural belt in Kuqa depression, Tarim basin. *Nat. Gas Geoscience.* **35**, 1532–1543 (2024).
- Yang, H. & Zhu, G. The condensate gas field geological characteristics and its formation mechanism in Tarim basin. *Acta Petrol. Sin.* **29**, 3233–3250 (2013).
- Zhu, G. et al. Geochemistry, origin and accumulation of continental condensate in the ultra-deep-buried cretaceous sandstone reservoir, Kuqa depression, Tarim basin, China. *Mar. Petrol. Geol.* **65**, 103–113. <https://doi.org/10.1016/j.marpetgeo.2015.03.025> (2015).
- Qiu, N. et al. New evidence on the neogene uplift of South Tianshan: constraints from the (U-Th)/He and AFT ages of borehole samples of the Tarim basin and implications for hydrocarbon generation. *Int. J. Earth Sci.* **101**, 1625–1643. <https://doi.org/10.1007/s00531-011-0745-0> (2012).
- Yang, K. et al. Structural deformation of the Northern monocline belt in the Kuqa depression and implications for the cenozoic uplift history of the South Tianshan mountains. *Tectonophysics* **857**, 229840. <https://doi.org/10.1016/j.tecto.2023.229840> (2023).
- Jia, C. Key scientific and technological problems of petroleum exploration and development in deep and ultra-deep formation. *J. China Univ. Petroleum (Edition Natrual Science)*. **47**, 1–12 (2023).
- Wang, B., Zhang, R., Ren, K., Luo, P. & Liu, C. Prediction of the lower limit of burial depth for effective reservoirs in the Dabei Kelasu deep structural belt of Kuqa depression. *Acta Petrolei Sinica.* **32**, 212–218 (2011).
- Wang, B., Qiu, N., Littke, R., Amberg, S. & Liu, Z. Petroleum system modelling in a compressional tectonic setting: the Eastern Kuqa depression, Tarim basin, Northwestern China. *J. Asian Earth Sci.* **249**, 105612. <https://doi.org/10.1016/j.jseas.2023.105612> (2023).
- Guo, X. et al. Constraining tectonic compression processes by reservoir pressure evolution: overpressure generation and evolution in the Kelasu thrust belt of Kuqa foreland basin, NW China. *Mar. Petrol. Geol.* **72**, 30–44. <https://doi.org/10.1016/j.marpetgeo.2016.01.015> (2016).
- Liu, L. et al. Synergistic deformation mechanisms and basin-mountain coupling of Kelasu structural belt in Kuqa depression. *Chin. J. Geol.* **57**, 61–72 (2022).
- Wei, G. et al. Structural reworking effects and new exploration discoveries of subsalt ultra-deep reservoirs in the Kelasu tectonic zone. *Nat. Gas. Ind.* **40**, 20–30 (2020).
- Liu, Z. et al. Influencing factor analysis on the fractured tight sandstone gas reservoir characteristics: a case study of Bozi 3 gas reservoir in the Tarim basin. *Front. Earth Sci.* **10**, 881934. <https://doi.org/10.3389/feart.2022.881934> (2022).
- Liang, D., Zhang, S., Zhao, M. & Wang, F. Hydrocarbon sources and stages of reservoir formation in Kuqa depression, Tarim basin. *Chin. Sci. Bull.* **47**, 62–70. <https://doi.org/10.1007/Bf02902820> (2002).
- Guo, S., Lyu, X. X. & Zhang, Y. Relationship between tight sandstone reservoir formation and hydrocarbon charging: A case study of a jurassic reservoir in the Eastern Kuqa depression, Tarim basin, NW China. *J. Nat. Gas Sci. Eng.* **52**, 304–316. <https://doi.org/10.1016/j.jngse.2018.01.031> (2018).
- Zhu, G. et al. Coupling relationship between natural gas charging and deep sandstone reservoir formation: A case from the Kuqa depression, Tarim basin. *Pet. Explor. Dev.* **36**, 347–357. [https://doi.org/10.1016/S1876-3804\(09\)60132-4](https://doi.org/10.1016/S1876-3804(09)60132-4) (2009).
- Ju, W. & Wang, K. A preliminary study of the present-day in-situ stress state in the Ahe tight gas reservoir, Dibeigasfield, Kuqa depression. *Mar. Petrol. Geol.* **96**, 154–165. <https://doi.org/10.1016/j.marpetgeo.2018.05.036> (2018).
- Graham, S. A., Hendrix, M. S., Wang, L. B. & Carroll, A. R. Collisional successor basins of Western China: impact of tectonic inheritance on sand composition. *Geol. Soc. Am. Bull.* **105**, 323–344. [https://doi.org/10.1130/0016-7606\(1993\)105<0323:Csbowc>2.3.Co;2](https://doi.org/10.1130/0016-7606(1993)105<0323:Csbowc>2.3.Co;2) (1993).
- Tian, J. et al. Discovery of well Bozi 9 and ultra-deep natural gas exploration potential in the Kelasu tectonic zone of the Tarim basin. *Nat. Gas. Ind.* **40**, 11–19 (2020).
- Liang, D., Zhang, S., Chen, J., Wang, F. & Wang, P. Organic geochemistry of oil and gas in the Kuqa depression, Tarim basin, NW China. *Org. Geochem.* **34**, 873–888. [https://doi.org/10.1016/S0146-6380\(03\)00029-9](https://doi.org/10.1016/S0146-6380(03)00029-9) (2003).
- Wan, J., Gong, Y., Zhuo, Q., Lu, X. & Huang, W. Fluid inclusion characteristics of the jurassic reservoir and hydrocarbon accumulation process in the Eastern Kuqa depression, Tarim basin. *J. Pet. Explor. Prod. Technol.* **13**, 523–541. <https://doi.org/10.1007/s13202-022-01570-6> (2023).
- Liang, Y. et al. Hydrocarbon accumulation model controlled by overpressure evolution in the Kelasu Thrust Belt of the Kuqa Depression, NW China. *Lithosphere* **2020**, 7352101 (2022).
- Qin, S., Dai, J. & Liu, X. The controlling factors of oil and gas generation from coal in the Kuqa depression of Tarim basin, China. *Int. J. Coal Geol.* **70**, 255–263. <https://doi.org/10.1016/j.coal.2006.04.011> (2007).

30. Zhao, S., Chen, W., Zhou, L., Zhou, P. & Zhang, J. Characteristics of fluid inclusions and implications for the timing of hydrocarbon accumulation in the cretaceous reservoirs, Kelasu thrust belt, Tarim basin, China. *Mar. Petrol. Geol.* **99**, 473–487. <https://doi.org/10.1016/j.marpetgeo.2018.10.041> (2019).
31. Aplin, A. C. et al. Combined use of confocal laser scanning microscopy and PVT simulation for estimating the composition and physical properties of petroleum in fluid inclusions. *Mar. Petrol. Geol.* **16**, 97–110. [https://doi.org/10.1016/S0264-8172\(98\)00079-8](https://doi.org/10.1016/S0264-8172(98)00079-8) (1999).
32. Aplin, A. C. et al. PVTX history of the North Sea's Judy oilfield. *J. Geochem. Explor.* **69**, 641–644. [https://doi.org/10.1016/S0375-6742\(00\)00066-2](https://doi.org/10.1016/S0375-6742(00)00066-2) (2000).
33. Liu, D. et al. Determination of trapping pressure and temperature of petroleum inclusions using PVT simulation software—a case study of lower ordovician carbonates from the Lunnan low uplift, Tarim basin. *Mar. Petrol. Geol.* **20**, 29–43. [https://doi.org/10.1016/S0264-8172\(03\)00047-3](https://doi.org/10.1016/S0264-8172(03)00047-3) (2003).
34. Chen, C. et al. Reconstruction of the evolution of deep fluids in light oil reservoirs in the central Tarim basin by using PVT simulation and basin modeling. *Mar. Petrol. Geol.* **107**, 116–126. <https://doi.org/10.1016/j.marpetgeo.2019.05.009> (2019).
35. Soave, G. Equilibrium constants from a modified Redlich-Kwong equation of state. *Chem. Eng. Sci.* **27**, 1197–1203. [https://doi.org/10.1016/0009-2509\(72\)80096-4](https://doi.org/10.1016/0009-2509(72)80096-4) (1972).
36. Deng, R., Chen, C., Shi, S. & Wang, Y. Fluid phase simulation and evolution of a condensate gas reservoir in the Tazhong uplift, Tarim basin. *Geofluids* **2019**, 8627698. <https://doi.org/10.1155/2019/8627698> (2019).
37. Deng, R., Wang, Y. & Chen, C. Fluid phase modeling and evolution of complex reservoirs in the Halahatang depression of the Tabei uplift, Tarim basin. *ACS Omega*. **7**, 14933–14943. <https://doi.org/10.1021/acsomega.2c00584> (2022).
38. Welte, D. H. & Yalcin, M. N. Basin modeling—A new comprehensive method in petroleum geology. *Org. Geochem.* **13**, 141–151. [https://doi.org/10.1016/0146-6380\(88\)90034-4](https://doi.org/10.1016/0146-6380(88)90034-4) (1988).
39. Hantschel, T. & Kauerauf, A. I. *Fundamentals of Basin and Petroleum Systems Modeling* (Springer, 2009).
40. Shi, S., Wang, Y., Chen, C., Liu, J. & Peng, P. Influence of tectonic evolution processes on burial, thermal maturation and gas generation histories of the Wufeng-Longmaxi shale in the Sichuan basin and adjacent areas. *Int. J. Coal Geol.* **295**, 104642. <https://doi.org/10.1016/j.coal.2024.104642> (2024).
41. Du, Z. & Wang, Q. Mesozoic and cenozoic uplifting history of the Tianshan region: insight from apatite fission track. *Acta Geol. Sin.* **81**, 1081–1101 (2007).
42. Cao, L. *The Hydrocarbon Accumulation Mechanism of Dabei-Kelasu Structural Zone in Kuqa Depression* (China University of Geosciences, 2010).
43. Song, X. *Cretaceous paleo-uplift Restoration and its Implications on Hydrocarbon Accumulation in the Kuqa Depression* (China University of Petroleum, 2018).
44. Xiao, Y. *Tectono-thermal Evolution of Northern Kuqa Depression and South Tien Shan* (China University of Petroleum, 2018).
45. Wang, L. et al. Terrestrial heat flow distribution in Kuqa foreland basin, Tarim, NW China. *Pet. Explor. Dev.* **32**, 79–83 (2005).
46. Lyu, C. et al. Evaluation of hydrocarbon generation using structural and thermal modeling in the thrust belt of Kuqa Foreland Basin, NW China. *Geofluids* **2020**, 8894030. <https://doi.org/10.1155/2020/8894030> (2020).
47. Tang, X., Yang, S. & Hu, S. Thermal and maturation history of jurassic source rocks in the Kuqa foreland depression of Tarim basin, NW China. *J. Asian Earth Sci.* **89**, 1–9. <https://doi.org/10.1016/j.jseaes.2014.03.023> (2014).
48. Zhang, Z. et al. Lacustrine to fluvial depositional systems: the depositional evolution of an intracontinental depression and controlling factors, lower cretaceous, Northern Tarim basin, Northwest China. *Mar. Petrol. Geol.* **126**, 104904. <https://doi.org/10.1016/j.marpetgeo.2021.104904> (2021).
49. Wei, L. et al. Reconstruction of the proto-type basin and tectono-paleogeographical evolution of Tarim in the cenozoic. *Front. Earth Sci.* **11**, 1095002. <https://doi.org/10.3389/feart.2023.1095002> (2023).
50. Li, X. et al. Reconstruction of the proto-type basin and tectono-paleogeography of Tarim block in the mesozoic. *Front. Earth Sci.* **11**, 1121428. <https://doi.org/10.3389/feart.2023.1121428> (2023).
51. Sun, Z. Methods for determining the type of different oil and gas reservoirs fluid. *Pet. Explor. Dev.* **23**, 69–75 (1996).
52. Xu, B. et al. Hydrocarbon phase state evolution and accumulation process of ultradeep permian reservoirs in Shawan Sag, Junggar basin, NW China. *Energy Fuels*. **37**, 12762–12775. <https://doi.org/10.1021/acs.energyfuels.3c01748> (2023).
53. Wang, J. et al. Fluid phase and hydrocarbon reservoir types of permian upper Urho formation in Shawan Sag, Junggar basin. *Lithologic Reservoirs*. **36**, 23–31 (2024).
54. Khavari-Khorasani, G., Dolson, J. C., Michelsen, J. & Part, I. K. The factors controlling the abundance and migration of heavy versus light oils, as constrained by data from the Gulf of Suez.: The effect of expelled petroleum composition, properties and petroleum system geometry. *Org. Geochem.* **29**, 255–282, doi: (1998). [https://doi.org/10.1016/S0146-6380\(98\)00152-1](https://doi.org/10.1016/S0146-6380(98)00152-1)
55. Chen, L., Zhu, G., Zhang, B., Wen, Z. & Wang, Y. Control factors and diversities of phase state of oil and gas pools in the Kuqa petroleum system. *Acta Geol. Sin.-Engl.* **86**, 484–496. <https://doi.org/10.1111/j.1755-6724.2012.00676.x> (2012).
56. Liu, K. et al. Deep petroleum accumulation models revisited: case studies from the Tarim basin. *Acta Geol. Sin.* **97**, 2820–2841 (2023).
57. Ren, Z. et al. Control effects of temperature and thermal evolution history of deep and ultra-deep layers on hydrocarbon phase state and hydrocarbon generation history. *Nat. Gas. Ind.* **40**, 22–30 (2020).
58. Di Primio, R., Dieckmann, V. & Mills, N. PVT and phase behaviour analysis in petroleum exploration. *Org. Geochem.* **29**, 207–222. [https://doi.org/10.1016/S0146-6380\(98\)00102-8](https://doi.org/10.1016/S0146-6380(98)00102-8) (1998).
59. Liu, J., Liu, K., Jiang, Z., Gui, L. & Li, F. Hydrocarbon accumulation processes in the Yangtake foldbelt, Kuqa foreland basin, NW China: insights from integrated basin modelling and fluid inclusion analyses. *J. Pet. Geol.* **41**, 447–466. <https://doi.org/10.1111/jpg.12716> (2018).
60. Tang, Y., Zhang, Y., Wei, C., Lv, Z. & Wu, Y. in *Green Energy, Environment and Sustainable Development* Vol. 38 *Advances in Transdisciplinary Engineering* (eds Wang, C. Q. et al.) 1096–1102 (IOS Press, Amsterdam, 2023).
61. Zhang, S., Zhang, B., Zhu, G., Wang, H. & Li, Z. Geochemical evidence for coal-derived hydrocarbons and their charge history in the Dabei gas field, Kuqa thrust belt, Tarim basin, NW China. *Mar. Petrol. Geol.* **28**, 1364–1375. <https://doi.org/10.1016/j.marpetgeo.2011.02.006> (2011).
62. Song, Y. et al. Differential hydrocarbon accumulation controlled by structural styles along the Southern and Northern Tianshan thrust belt. *Acta Geol. Sin.-Engl. Ed.* **87**, 1109–1119. <https://doi.org/10.1111/1755-6724.12113> (2013).
63. Zhao, M. et al. Characteristics and distribution law of hydrocarbon accumulation in Kuqa foreland basin. *Acta Petrolei Sinica*. **36**, 395–404 (2015).
64. Zhuo, Q. et al. Hydrocarbon migration through salt: evidence from Kelasu tectonic zone of Kuqa foreland basin in China. *Carbonates Evaporites*. **29**, 291–297. <https://doi.org/10.1007/s13146-013-0177-y> (2013).
65. Batalin, O. & Vafina, N. Condensation mechanism of hydrocarbon field formation. *Sci. Rep.* **7** <https://doi.org/10.1038/s41598-017-10585-7> (2017).
66. Zhuo, Q. et al. The salt chimney effect: delay of thermal evolution of deep hydrocarbon source rocks due to high thermal conductivity of evaporites. *Geofluids* **16**, 440–451. <https://doi.org/10.1111/gfl.12162> (2016).
67. Zhao, W. et al. Gas systems in the Kuche depression of the Tarim basin: source rock distributions, generation kinetics and gas accumulation history. *Org. Geochem.* **36**, 1583–1601. <https://doi.org/10.1016/j.orggeochem.2005.08.016> (2005).
68. Chen, C., Wang, Y., He, Z., Li, J. & Wang, Y. Influence of gas washing and oil mixing on the phase behavior and physical properties of cambrian light oils in the Tazhong uplift, Tarim basin. *Energies* **17**, 5494 (2024).

69. Losh, S., Cathles, L. & Meulbroek, P. Gas washing of oil along a regional transect, offshore Louisiana. *Org. Geochem.* **33**, 655–663. [https://doi.org/10.1016/S0146-6380\(02\)00025-6](https://doi.org/10.1016/S0146-6380(02)00025-6) (2002).
70. Lei, W., Chen, D., Cheng, M., Cai, C. & Wang, Q. Combined use of petroleum inclusion analysis, PVT simulation, and basin modeling for reconstruction of deep fluid phase evolution in condensate gas reservoirs. *Mar. Petrol. Geol.* **171**, 107210. <https://doi.org/10.1016/j.marpetgeo.2024.107210> (2025).
71. Wu, F. et al. Types of hydrocarbon migration pathways and its controlling effects on hydrocarbon distribution in Tarim basin. *Acta Petrolei Sinica.* **30**, 332–341 (2009).
72. Song, Y. et al. Dominant factors of hydrocarbon distribution in the foreland basins, central and Western China. *Pet. Explor. Dev.* **39**, 265–274 (2012).
73. Qin, P., Zhong, D., Su, C., Mo, T. & Tang, Y. Effect of the internal plastic deformation of salt structures on the lithologic succession of evaporites: A case study on the palaeogene Kumugeliemuqun formation, Kelasu thrust belt, Kuqa depression, Tarim basin. *J. Petrol. Sci. Eng.* **208**, 109559. <https://doi.org/10.1016/j.petrol.2021.109559> (2022).
74. He, W. et al. The effects of salt flow on the cross-section restoration of salt-bearing fold-and-thrust belts: an example from the Kuqa depression. *J. Struct. Geol.* **167**, 104795. <https://doi.org/10.1016/j.jsg.2023.104795> (2023).
75. Wang, Q., Zhang, L., Lu, X., Zhou, L. & Wang, R. Hydrocarbon accumulation types and distribution prediction of Western section of frontal uplift of Kuqa foreland basin. *Acta Petrolei Sinica.* **44**, 730–747 (2023).

Acknowledgements

This work was supported by National Natural Science Foundation of China program (Grant Nos. 42273053, 42203054, and 42402136), and the Theory of Hydrocarbon Enrichment under Multi-Spheric Interactions of the Earth (Grant No. THEMSIE04010104). We also thank Simon George from Macquarie University, Australia, for constructive comments and editing of the manuscript. This is contribution No.IS-3654 from GIGCAS.

Author contributions

Z.H. drafted the main manuscript text. C.C., S.S., and M.L. conducted some of the simulation work. C.W., T.M., and N.D. provided fluid compositions data. C.C. and Y.W. improved the structure and language. All authors reviewed the manuscript.

Declarations

Competing interests

The authors declare no competing interests.

Additional information

Supplementary Information The online version contains supplementary material available at <https://doi.org/10.1038/s41598-025-03736-8>.

Correspondence and requests for materials should be addressed to C.C. or Y.W.

Reprints and permissions information is available at www.nature.com/reprints.

Publisher's note Springer Nature remains neutral with regard to jurisdictional claims in published maps and institutional affiliations.

Open Access This article is licensed under a Creative Commons Attribution-NonCommercial-NoDerivatives 4.0 International License, which permits any non-commercial use, sharing, distribution and reproduction in any medium or format, as long as you give appropriate credit to the original author(s) and the source, provide a link to the Creative Commons licence, and indicate if you modified the licensed material. You do not have permission under this licence to share adapted material derived from this article or parts of it. The images or other third party material in this article are included in the article's Creative Commons licence, unless indicated otherwise in a credit line to the material. If material is not included in the article's Creative Commons licence and your intended use is not permitted by statutory regulation or exceeds the permitted use, you will need to obtain permission directly from the copyright holder. To view a copy of this licence, visit <http://creativecommons.org/licenses/by-nc-nd/4.0/>.

© The Author(s) 2025, corrected publication 2026